# Atmospheric $H_2$ observations from the NOAA Cooperative Global Air Sampling Network

Gabrielle Pétron[1,2], Andrew M. Crotwell[1,2], John Mund[1,2], Molly Crotwell[1,2], Thomas Mefford[1,2], Kirk Thoning[2], Bradley Hall[2], Duane Kitzis[1,2], Monica Madronich[1,2], Eric Moglia[1,2], Donald Neff[1,2], Sonja Wolter[1,2], Armin Jordan[3], Paul Krummel[4], Ray Langenfelds[4], John Patterson[5]

*Correspondence to*: Gabrielle Pétron (gabrielle.petron@noaa.gov)

1. Cooperative Institute for Research in Environmental Sciences, CU Boulder, USA
2. NOAA Global Monitoring Laboratory, Boulder, USA
3. Max-Planck-Institute for Biogeochemistry (MPI-BGC), Jena, Germany
4. Commonwealth Scientific and Industrial Research Organisation - Environment, Aspendale, Australia
5. Department of Earth System Science, University of California, Irvine, USA

**Abstract.** The NOAA Global Monitoring Laboratory (GML) measures atmospheric hydrogen ($H_2$) in grab-samples collected weekly as flask pairs at over 50 sites in the Cooperative Global Air Sampling Network. Measurements representative of background air sampling show higher $H_2$ in recent years at all latitudes. The marine boundary layer (MBL) global mean $H_2$ was 552.8 ppb in 2021, 20.2 ±0.2 ppb higher compared to 2010. A 10 ppb or more increase over the 2010-2021 average annual cycle was detected in 2016 for MBL zonal means in the tropics and in the Southern Hemisphere. Carbon monoxide measurements in the same air samples suggest large biomass burning events in different regions likely contributed to the observed interannual variability at different latitudes. The NOAA $H_2$ measurements from 2009 to 2021 are now based on the World Meteorological Organization Global Atmospheric Watch (WMO GAW) $H_2$ mole fraction calibration scale, developed and maintained by the Max-Planck Institute for Biogeochemistry (MPI-BGC), Jena, Germany. GML maintains eight $H_2$ primary calibration standards to propagate the WMO scale. These are gravimetric hydrogen-in-air mixtures in electropolished stainless steel cylinders (Essex Industries, St. Louis, MO), which are stable for $H_2$. These mixtures were calibrated at the MPI-BGC, the WMO Central Calibration Laboratory (CCL) for $H_2$, in late 2020 and span the range 250-700 ppb. We have used the CCL assignments to propagate the WMO $H_2$ calibration scale to NOAA air measurements performed using Gas Chromatography-Helium Pulse Discharge Detector instruments since 2009. To propagate the scale, NOAA uses a hierarchy of secondary and tertiary standards, which consist of high-pressure whole air mixtures in aluminum cylinders, calibrated against the primary and secondary standards respectively. Hydrogen at the ppb-level has a tendency to increase in aluminum cylinders over time. We fit the calibration histories of these standards with 0-2nd order polynomial functions of time and use the time-dependent mole fraction assignments on the WMO scale to reprocess all tank air and flask air $H_2$ measurement records. The robustness of the scale propagation over multiple years is evaluated with the regular analysis of target air cylinders and with long-term same air measurement comparison efforts with WMO GAW partner laboratories. Long-term calibrated, globally distributed and freely accessible measurements of $H_2$ and other gases and isotopes continue to be essential to track and interpret regional and global changes in the atmosphere composition. The adoption of the WMO $H_2$ calibration scale and subsequent reprocessing of NOAA atmospheric data constitute a significant improvement in the NOAA $H_2$ measurement records.

## 1 Introduction

High quality and sustained observations are essential to track and study changes in atmospheric trace gas distributions. Ambient air measurement programs for trace gases provide objective data to track air pollution levels [Oltmans and Levy, 1994; Thomson et al., 2004; Tørseth et al., 2012; Schultz et al., 2015; Cooper et al., 2020; WMO, 2022], to study how a mix of sources (and sinks) impact the air composition [Ciais et al., 1995; Pétron et al., 2012; Langenfelds et al., 2002; Brito et al., 2015] and to constrain and evaluate fluxes and their trends at scales of interest [von Schneidemesser et al., 2010; Simpson et al., 2012; Propper et al., 2015; Montzka et al., 2018; Friedlingstein, 2022; Heiskanen et al., 2022; Storm et al., 2023].

$H_2$ is a trace gas in the Earth's atmosphere and its abundance can indirectly impact climate and air quality. The analysis of $H_2$ measurements in firn air collected in Antarctica reveal that $H_2$ levels in the high-latitude southern hemisphere grew by some 70% (330 to 550 ppb, 1 ppb = 1 mole of gas per billion ($10^9$) moles of air) over the 20th century [Patterson et al., 2021; 2023]. Greenland firn air covers less depth and time but results are consistent with a 30% increase in high-latitude northern hemisphere $H_2$ from 1950 to the late 1980s [Patterson et al., 2023]. Growing emissions related to fossil fuel burning most likely were behind this rise in $H_2$ [Patterson et al., 2021]. Results also show that $H_2$ in both polar regions leveled off after the 1990s [Patterson et al., 2021, 2023].

$H_2$ has been viewed as a potential low or zero carbon energy carrier for close to five decades [Yap and McLellan, 2023]. Since 2020 there has been renewed interest in the hydrogen economy [Yap and McLellan, 2023] spurred by a rise in announcements of public and private projects to produce low carbon $H_2$, also referred to as "blue" $H_2$ produced from natural gas with carbon capture, utilization and storage, or "green" $H_2$ produced using renewable energy [Hydrogen Council and McKinsey & Company, 2023]. In 2021, $H_2$ global demand was over 94 million tonnes or 2.5 % of global final energy consumption [IEA, 2022]. This demand was almost entirely driven by refineries and a few industries (ammonia, methanol and steel) and $H_2$ production almost entirely relied on fossil fuels with unabated emissions ("gray $H_2$", [IEA, 2022]). As of December 2023, over 1,400 announced projects globally (worth US$ 570 billion) are anticipated to increase the global $H_2$ production capacity by 45 million tonnes through 2030 [Hydrogen Council and McKinsey & Company, 2023].

Studies of the potential short-term and long-term climate impacts of increased $H_2$ production and use have called for more research to better understand the current and future $H_2$ supply chain and end-use emissions of $H_2$ and GHGs [Ocko and Hamburg, 2022; Longden et al., 2022; de Kleijne et al., 2022; Bertagni et al., 2022; Warwick et al., 2023]. Global, high quality and sustained atmospheric measurements of $H_2$ can provide independent information to document its distribution and study its sources and sinks and how they may change.

The National Oceanic and Atmospheric Administration (NOAA) Cooperative Global Air Sampling Network comprises over 50 surface and mostly remote sites (https://gml.noaa.gov/ccgg/flask.html). At each site and on a weekly basis, local partners collect air in two 2.5-L glass flasks, and then return the flasks to the NOAA Global Monitoring Laboratory (GML) in Boulder, Colorado, USA, for measurements of major long-lived greenhouse gases, carbon dioxide ($CO_2$), methane ($CH_4$), nitrous oxide ($N_2O$), sulfur

hexafluoride ($SF_6$), as well as carbon monoxide (CO) and hydrogen ($H_2$) [Conway et al., 1994; Novelli et al., 1999; Dlugokencky et al., 2009]. The network is a contributor to the World Meteorological Organization (WMO) Global Atmospheric Watch (GAW) Programme, which promotes and coordinates international scientific efforts and free access to long-term atmospheric observations [WMO, 2022].

CO and $H_2$ are important trace gases that share sources with $CO_2$ and $CH_4$ (fossil fuel burning, biofuel burning and wildfires). Reaction with hydroxyl radicals (OH) is the main sink for $CH_4$ and CO and an important sink for $H_2$. Both $H_2$ and CO are also produced during the chemical oxidation of $CH_4$ and nonmethane hydrocarbons. Soil uptake by bacteria accounts for 75% of the total $H_2$ sink. $H_2$ and CO have much shorter atmospheric lifetimes than $CO_2$ and $CH_4$: 2-3 months for CO and close to 2 years for $H_2$. The $H_2$ global mean atmospheric lifetime is largely driven by the soil sink strength. The $H_2$ lifetime related to the oxidation by OH is estimated to be 8-9 years [Price et al., 2007; Warwick et al., 2022].

Novelli et al. [1991, 1992] reported for NOAA on testing the air sampling approach (flask type, stopcock fitting, wet/dry air, untaped versus taped glass flasks to minimize direct sunlight exposure) and an analytical instrument consisting of a gas chromatograph (GC) and a reduction gas analyzer (RGA, from Trace Analytical Inc., California) that could measure both CO and $H_2$. Around that time, other laboratories had also adopted the technique for CO and $H_2$ measurements in discrete air samples or in situ. Khalil and Rasmussen [1989, 1990] reported on $H_2$ measurements of whole air samples collected weekly in triplicate electropolished stainless steel flasks between October 1985 and April 1989 at the four NOAA atmospheric baseline observatories (Point Barrow, Mauna Loa, Samoa, South Pole), Cape Meares, Oregon, Cape Kumukahi, Hawaii and at the Cape Grim Observatory, Tasmania. These measurements showed that, contrary to $CO_2$, $CH_4$, $N_2O$ and CO, background air $H_2$ levels were higher in the Southern Hemisphere (SH) than in the Northern Hemisphere (NH). 1985-1987 monthly mean observed $H_2$ ranged between 500-520 ppb at the South Pole and between 455 and 520 ppb at Point Barrow. $H_2$ exhibited a strong seasonal cycle at extratropical latitudes especially in the NH and the seasonal cycles in both hemispheres were offset by 1-2 months only.

In 1995, $H_2$ mole fraction calibration standards were prepared gravimetrically in aluminum cylinders (Scott Marrin Inc., Riverside, CA) and five of them (spanning 485-603 ppb) were used to define the NOAA $H_2$ X1996 calibration scale. Working standards used in the NOAA flask analysis laboratory between 1988 and 1996 were reassigned $H_2$ mole fractions and flask air measurements were reprocessed to be on the X1996 scale. Novelli et al. [1999] described the early NOAA $H_2$ measurements and reported $H_2$ time series starting in the late 1980s or early 1990s (depending on the site) for 50 sites in the NOAA Cooperative Global Air Sampling Network.

Simmonds et al. [2000] reported in-situ high-frequency GC-RGA3 measurements of $H_2$ at the Mace Head baseline atmospheric monitoring station on the Atlantic coast of Ireland for the 1994-1998 period. They found that the background air at Mace Head had lower monthly mean $H_2$ (470-520 ppb) than background air masses measured at the Cape Grim observatory (510-530 ppb) from July to April. Some of the 40 min $H_2$ observations showed 10-200 ppb short-term $H_2$ enhancements above baseline levels. The authors derived an estimate of European emissions with an inverse model of enhanced $H_2$ in air masses impacted by upwind sources of pollution. They also observed that nighttime measurements in low wind conditions

reflected local depletion of $H_2$. The authors derived variable mean deposition velocities and found that the $H_2$ soil sink was likely a process that occurred year-round in the area.

After 1996 and until 2008, the NOAA $H_2$ measurement program used successive working standards that were assigned based on GC-RGA measurements against the previous standards. With hindsight, the NOAA X1996 calibration scale transfer and the early NOAA $H_2$ measurements had several limitations which are briefly described below and in more detail in the Supplementary Information section S1.

By the late 1990s, same air or colocated air sample measurement comparison between NOAA and the Commonwealth Scientific and Industrial Research Organisation (CSIRO) for the Cape Grim Observatory and Alert, Canada, flask air analyses showed an increasing bias for $H_2$ between the two laboratories [Masarie et al., 2001; Francey et al., 2003]. Further laboratory tests by several WMO/GAW measurement laboratories revealed the RGA detector response was non linear and required frequent calibration. Additionally measurement laboratories found that the $H_2$ mole fraction for air standards, especially those stored in high pressure aluminum cylinders, could drift at rates of a few parts per billion (ppb) to tens of ppb per year [Novelli et al., 1999; Masarie et al., 2001; Jordan and Steinberg, 2011].

To address these compounding issues, in 2008 NOAA GML tested a new analytical instrument: a gas chromatograph with a pulse discharge helium ionization detector (GC-HePDD) [Wentworth et al., 1994]. The technique showed very good performance with a stable and linear response over the 0-2000 ppb range and it was adopted for the calibration scale propagation and flask air analysis in 2009 [Novelli et al., 2009]. Around that time GML also began testing electropolished stainless steel cylinders (Essex Industries, St. Louis, MO) filled with dry air for stability.

In 2007-2008, GML prepared six new gravimetric air mixtures in electropolished stainless steel cylinders spanning 250-600 ppb $H_2$. At that time, the new gravimetric mixtures differed by about +20 ppb compared to two $H_2$ secondary standards values assigned on the NOAA $H_2$ X1996 scale. For the next decade, GML kept using the NOAA X1996 calibration scale while also conducting routine measurements of the $H_2$ secondary standards against the 2007/2008 gravimetric mixtures.

The GC-HePDD $H_2$ measurements on the NOAA $H_2$ X1996 scale remained biased compared to GAW partner measurements and the NOAA $H_2$ data from the global network flasks were not released publicly after 2005. SI sections S1-3 and SI Table 1 provide additional information on issues impacting the 1988-2008 NOAA $H_2$ measurements on RGAs, and related information from the CSIRO and Max-Planck Institute for Biogeochemistry (MPI-BGC) $H_2$ measurement programs. The more precise and better calibrated NOAA $H_2$ measurement records date back to 2009/2010 and are the main focus of this paper.

In Fall 2020, GML initiated an effort to 1) adopt the WMO MPI X2009 $H_2$ calibration scale [Jordan and Steinberg, 2011] for future measurements and 2) convert GML $H_2$ measurements made on GC-HePDD instruments (beginning in late 2009) to that scale. This paper describes the MPI X2009 $H_2$ calibration scale propagation within GML and the revised measurements from the NOAA Cooperative Global Air Sampling Network flask air samples analyzed since late 2009. We show very good agreement for the reprocessed NOAA $H_2$ data for different WMO GAW measurement comparison efforts. The revised NOAA GML flask air $H_2$ dry air mole fraction measurement records for 70 surface sites from 2009-2021

are publicly available [Pétron et al., 2023a]. This new dataset complements other WMO GAW $H_2$ measurement datasets and provides reliable observational constraints for the study of atmospheric $H_2$ global distribution and budget since 2009. Future NOAA $H_2$ dataset updates will be released as we use continued calibration results to reliably track the drift in standards and revise their assignments.

## 2 Adoption of the WMO MPI X2009 $H_2$ calibration scale

To infer fluxes and trends from atmospheric measurements, scientists need to reliably detect small temporal and spatial gradients in the abundance of trace gases. This requires comparable data across time and across monitoring networks to ensure biases are minimized and do not influence interpretation. The use of a common calibration scale among measurement laboratories ensures data are traceable to a common reference. It is the first step in preventing biases that could stem from using different references.

In this section, we introduce the NOAA GML $H_2$ calibration standard hierarchy and describe the adoption of the WMO MPI X2009 $H_2$ scale. Calibration at GML is based on a hierarchy of standards (primary, secondary, tertiary) and a dedicated $H_2$ calibration system used to transfer the scale from the primary standards to secondary and tertiary standards. An important quality assurance procedure within GML is the routine measurement of dedicated quality control cylinders (referred to as "Target" tanks) to track instrument performance. Results are discussed in relation to the uncertainty of the flask air analysis systems and consistency of the MPI X2009 $H_2$ scale implementation.

### 2.1 NOAA GML $H_2$ primary standards

In 2007-2008, six mixtures of $H_2$ in dry air were prepared gravimetrically at GML in electropolished stainless steel 34L cylinders ([Novelli et al., 2009], and Table 1). The highest $H_2$ mole fraction tank developed a leak and was lost. The remaining set of five standards covered the range 250 ppb to 600 ppb for $H_2$. Three standards in electropolished stainless steel cylinders were added in 2019 to extend the upper limit of the calibration range to 700 ppb $H_2$ and evaluate the stability of the initial set over the intervening years. In 2020, these eight standards were designated as NOAA GML's highest level $H_2$ standards. We refer to them as the NOAA $H_2$ primary standards throughout this document even though they are not used to independently define the scale.

The eight primary standards were analyzed by the WMO Central Calibration Laboratory (CCL) for $H_2$ hosted by the MPI-BGC in Jena, Germany, on their GC-PDD system in November 2020. The results listed in Table 1 are reported on the MPI X2009 $H_2$ calibration scale [Jordan and Steinberg, 2011]. The CCL uncertainty estimates listed in Table 1 refer to the standard deviation of the 25-32 discrete $H_2$ measurements made for each standard. Until they are recalibrated by the CCL, we add an 0.5 ppb 1-sigma uncertainty to these assignments. This is the currently reported CCL reproducibility for their GC-PDD $H_2$ measurements. It accounts for potential longer term uncertainty in calibration results that would not be evident in the standard deviations of measurements made close in time.

### 2.2 MPI X2009 $H_2$ calibration scale transfer

GML has separate, dedicated analytical systems for scale propagation and flask air analyses. Novelli et al. [2009] describe the GC-HePDD instruments and the operating parameters in detail. GML has used three GC-HePDD instruments so far. Each is identified by a unique internal instrument identification code: H9 for tank calibrations and H8 and H11 for flask analyses. The GC-HePDD instruments' responses are linear (within 0.3%) up to 2000 ppb. They are configured for ppb level sensitivity and calibrated over the 200-700 ppb range, which is optimal for global and regional background air analysis.

The GML $H_2$ primary standards are used to periodically calibrate the H9 instrument response for the analysis and value assignment of lower level standards. The stability and longevity of the primary standards are critical to ensure the consistency of the GML $H_2$ measurements over long periods of time as required for trend analysis.

The $H_2$ secondary and tertiary standards used in GML are whole air mixtures in high pressure aluminum cylinders (Luxfer USA). Most were filled at the GML standard air preparation facility at the Niwot Ridge mountain research station using a Rix Industries (Benicia, CA) SA6 oil-free compressor [Kitzis, 2017]. Two additional tertiary standards were purchased from Scott Marrin. All GML tank air mixtures have a unique combination of an alphanumeric cylinder ID and a fill code letter (A-Z) tied to a fill date.

Aluminum tanks are known to be unstable for storing $H_2$ in air standards [Jordan and Steinberg, 2011]. Therefore regular analyses of standards on the tank calibration system are critical for quantifying drift to allow a time dependent value assignment on the MPI X2009 $H_2$ calibration scale.

GML uses python software developed in-house to record calibration data, compute mole fractions, and evaluate the stability of $H_2$ mole fractions over time. All mole fraction assignments and associated drift coefficients for standards used to propagate a calibration scale are stored in a database table that can be accessed by the data processing software. The software allows for 0-2nd order polynomial drift functions. As new calibration results are available, the drift correction and assignment for a particular tank ID and fill code are revised as needed and the affected data are reprocessed.

#### 2.2.1 Scale transfer: 2009-2019

From 2007 through mid-April 2019, the $H_2$ tank air calibration on the H9 instrument was conducted using a single standard gas (primary or secondary standard) to calibrate the "unknown" (secondary or tertiary) standards. A tank calibration event consisted of alternating injections of the reference/standard gas and the "unknown" tank air with typically seven or more unknown air injections. The first aliquot in a multi injection measurement sequence on H9 is often slightly biased (due to subtle timing differences with the regulator flush cycle) and is not used. The ratio of the $H_2$ peak height for each valid "unknown" air injection and the mean peak height of two bracketing reference gas injections (or sometimes only one preceding or following reference gas injection) is multiplied by the reference/standard gas known $H_2$ mole fraction to calculate the "unknown" air injection mole fraction. Results for a tank air calibration event are defined by the mean and the standard deviation of the calculated $H_2$ mole fractions for five or more retained unknown air injections. Typically, the standard deviation for a tank air calibration event on H9 is less than 1 ppb.

Prior to the 2023 GML $H_2$ data reprocessing, GML used peak area for the GC-HePDD as described in Novelli et al. [1999]. However, we saw that for some Helium carrier gas tanks (Airgas Ultra High Purity, (99.999% purity), the $H_2$ chromatogram peak had a tail or a noisy baseline. Since the $H_2$ peak height was less affected, we use peak height ratios for all GC-HePDD measurements. In 2023, GML switched to Matheson Research Grade Helium carrier gas for the GC-HePDDs (99.9999% purity).

The calibration results for the two $H_2$ secondary standards used between 2009 and Arpil 2019 are plotted in Figure 1 and final assignments are listed in SI Table 2. A small non zero y-intercept for H9 (see next section) likely explains the biased results for CC119811 against the lowest primary standards (SX-3558 and SX-3543). Results against SX-3558 were not used for value assigning either secondary standards and results against SX-3543 were not used for CC119811.

CA03233 was stable for $H_2$ over its time of use and has an assignment of 502.8 ppb $H_2$. $H_2$ in CC119811 exhibited a small linear drift and its value assignment is time dependent with a growth rate of 2 ppb/yr. Between 2009 and 2019, these two secondary standards were used on H9 to calibrate seventeen $H_2$ tertiary standards used in the NOAA flask analysis laboratory.

### 2.2.2 Scale transfer: 2019-present

Beginning in April 2019, GML transitioned H9 to use a multi-point calibration strategy to better define the instrument response. The eight $H_2$ primary standards are measured relative to a reference air tank (CC49559, filled with ambient Niwot Ridge dried air) to calibrate the instrument response. A multi-standard response calibration episode for H9 involves the alternating injections from the reference air tank and each primary standard. Each standard is injected 8 times alternating with reference air aliquots. The entire response calibration sequence takes close to 15 hours. GML has performed an H9 instrument response calibration 2 to 3 times a year, followed by tank calibrations over a 10-14 day period each time.

The H9 instrument response function is calculated as the best linear fit to the primary standards' mean normalized chromatogram peak heights and their CCL $H_2$ mole fraction assignments. H9 calibration curves are assumed to be valid for several weeks during which time other air cylinders are analyzed relative to the same reference tank.

Between April 2019 and December 2022, the H9 instrument response was determined relative to the primary standards nine times. Figure 2a shows the deviations of the H9 linear response functions from the line defined by computing the mean value for the intercept and slope of the 2019-2022 response functions. The instrument response has remained stable within +/- 1 ppb over this time period over the range 200-700 ppb. The residuals to each linear fit over this time period are all within the -0.6 ppb to 0.5 ppb range (Figure 2b). The linear fit y-intercept ranges between 3.9 and 5.5 ppb (not shown). Prior to 2019, we assumed a zero intercept for the H9 one point calibration. If we assume a y-intercept around 5 ppb was more likely, it is possible the pre-2019 H9 measurements (with 1 point calibration) were biased by ~1% of the difference between the tank air and the standard $H_2$ mole fractions. We do not correct for this potential bias at this time.

Since April 2019, a tank air measurement sequence on H9 has consisted of 7 tank air injections, each bracketed by reference air injections. The peak heights for the first injections of reference air and tank air can have a small low bias and are not used. The normalized peak heights for the valid tank air injections are converted to $H_2$ mole fractions using the most recent H9 response function. The average and standard deviation of the retained injection $H_2$ mole fractions are stored in a database table.

### 2.2.3 $H_2$ standards and calibration approach for the flask air analysis system

$H_2$ in flask air samples is measured in addition to long-lived GHGs ($CO_2$, $CH_4$, $N_2O$, $SF_6$) and CO by the Measurement of Atmospheric Gases that Influence Climate Change (MAGICC) system in the NOAA GML Boulder laboratory. Until mid 2019, GML operated two nearly-identical automated flask air analytical systems: MAGICC-1 (1997-2019) and MAGICC-2 (2003-2014). Since mid-2019, GML has used a new MAGICC-3 system. This new system improved analytical techniques for $CO_2$, $CH_4$, $N_2O$, and CO but continues to use the same GC-HePDD instruments from the older systems.

Two GC-HePDD instruments have been used for hydrogen analysis on the three flask air analysis systems since 2009: H8 (MAGICC-2: 2009-2014 and MAGICC-3: August 2019-September 2020) and H11 (MAGICC-1: 2010-July 2019 and MAGICC-3: September 2020-present).

On MAGICC-1 and MAGICC-2, the $H_2$ instrument response was calibrated using a single tertiary standard (measured before and after each sample aliquot), similar to the original 1 point calibration approach used on H9.

Out of 17 $H_2$ tertiary standards used during that time, 3 were used for more than 14 months and 14 displayed $H_2$ growth over time. Figure 3 shows the calibration histories for H8 and H11 tertiary standards and their start/deployment dates. For each tertiary standard, assigned mole fractions, drift coefficients, and estimated uncertainties are stored in a database (SI Table 2). The uncertainty reported in SI Table 2 is empirically derived and based on the standard calibration history and the standard deviation of the residuals to the best fit (the assignment). The python code that calculates a secondary or tertiary standard assignment uses a 0.5 ppb 1-sigma H9 reproducibility uncertainty which is added in quadrature to the measurement episode standard deviation to account for longer term uncertainties not evident in the standard deviation of the n-aliquots. We do not formally include an uncertainty for the secondary standard assignments. The H9 reproducibility term is based on the mean of the standard deviation of residuals to the fit for the calibration histories of secondary standards and target tanks over the period 2008-2022 (see section 2.3.1).

The 17 tertiary standards used successively on the flask analysis systems between 2009 and 2019 introduce time dependent issues due to the variable rate of $H_2$ drift in aluminum tanks and the tank calibration histories. Some of the tertiary standards only have pre-deployment calibration results which do not assess drift during use and other standards have calibration results during their time in use but do not have post deployment calibrations that may help us evaluate the drift rate for the last couple of weeks or months of use (SI Table 2, notes in column “N”). Three standards exhibited an increased drift rate towards the end of their life that we did not capture with their infrequent calibrations on H9. This change in drift behavior was observed as increasing biases for measurements of target air tanks and daily test air flasks (see section 3.2). We have applied offline mole fraction corrections to the flask air analysis $H_2$ results to

correct for the end of use drift increase for these  three tertiary standards , and the standards' assignment uncertainty is larger for these time periods (SI Table 2).

Since August 2019, the MAGICC-3 system operates with a GC-HePDD for $H_2$, new optical analyzers for $CO_2$, $CH_4$ (CRDS, Picarro), CO and $N_2O$ (QC-TILDAS, Aerodyne), and a GC-ECD for $SF_6$. The responses of the instruments are calibrated at the same time using a single set of 11 standards spanning a range of mole fractions for the six trace gases. The MAGICC-3 standards were filled at the Niwot Ridge standard air preparation facility on a few different days between December 2017 and May 2018. Their $H_2$ mole fractions are regularly measured on H9 against the GML $H_2$ primary standards.

For the MAGICC-3 instrument response calibration, the eleven standards are analyzed sequentially relative to an uncalibrated reference air tank (filled at Niwot Ridge). Air from each standard is injected 6 times alternating with the reference air. This entire sequence takes close to 17 hours. The first injection of each standard is often biased low by about 2 ppb for $H_2$ due to timing issues at the start of each standard sequence and only the remaining 5 injections are used to obtain the average normalized peak height "signal" for each standard.

For $H_2$, a subset of 8 of the 11 MAGICC-3 standards are used to determine the GC-HePDD response. The time-dependent $H_2$ value assignment for each standard was derived from 8 or 9 calibration events on H9 between June 2018 and December 2022 (SI Table 3, SI Figures 1 and 2). We plan on analyzing the MAGICC-3 standards 2 to 3 times a year going forward. The standards' $H_2$ assignments will be revised as needed. The three cylinders that are not used exhibit complex $H_2$ growth that is not well captured with periodic calibration episodes and a linear or quadratic fit.

The time between MAGICC-3 instrument response calibration sequences was 2 weeks for the first 3 months of service and it has been increased to 4-5 weeks as we found the results to be quite stable. A reference air cylinder will last 9 to 12 months on MAGICC-3. When the MAGICC-3 reference air cylinder is changed (pressure close 250 psia), a new instrument response calibration episode is done with the new reference air cylinder before flask air samples are analyzed.

For the asynchronous calibration to stay valid for up to 5 weeks requires the reference gas composition for the six measured gases to be stable between successive calibration episodes. This has been true so far except for one reference air cylinder for which a small time dependent $H_2$ correction was applied between two instrument response calibration dates (see SI Figure 3 and more details in SI section S4).

### 2.3 Calibration scale transfer quality assurance

GML target air tanks are dedicated air mixtures used for measurement quality control over multiple years. Most are high pressure aluminum cylinders filled at the Niwot Ridge standard preparation facility. The analysis of target air helps us evaluate the robustness of the calibration scale transfer, and the consistency of measurements over time and also between different analytical systems. In a perfect program, we should be able to reproduce a measurement result for a target air tank every time. As noted earlier, however, the reality is more complicated as $H_2$ tends to grow with time in aluminum cylinders. Tracking many aluminum cylinders provides a diverse history of behaviors (stable, or linear vs non-linear drift), and aids in the understanding of similar cylinders used for calibration.

### 2.3.1 Calibration system (H9) Target air tanks

Some GML target air cylinders are used exclusively to evaluate the stability and performance of the H9 measurements. Other target air cylinders are analyzed on H9 and in the flask air analysis laboratory on the H8 and H11 instruments to evaluate the scale transfer.

While $H_2$ has been increasing in most of our target air tanks, eleven H9 target air tanks have shown either stable $H_2$ or a linear rate of increase less than 1 ppb/yr. Figure 4 shows the calibration histories for these tanks as well as the residuals from the best fit for each tank. Table 2 has a list of these target tanks and several others binned by linear drift rate. More details for target tanks are in SI Table 4. For each bin, the standard deviation of the residuals (differences of the H9 calibration results minus the best fit values) is below 0.5 ppb. The standard deviation of all linearly drifting target tanks residuals binned together is 0.4 ppb.

Results for tanks with stable or very slowly drifting $H_2$ indicate that between 2008 and 2021, the scale transfer on H9 has low uncertainty ( < 1 ppb). We have eleven other target tanks for which the best fit to their calibration history is a quadratic function (SI Figure 4 and SI Table 4). The standard deviation of these tanks' residuals binned together is 0.7 ppb. The current set of H9 target air tank results show that residuals for higher mole fraction (>650 ppb) tanks have a larger standard deviation (0.5-0.8 ppb, SI Figure 4d).

Some tanks that were analyzed soon after fill and over several years show a rapid and large initial growth in $H_2$ (in the first 0.5-2 years after fill). In this scenario, the residuals to a best linear or quadratic fit of the full calibration history will be larger and will likely not capture the tank time-dependent $H_2$ assignment as accurately. For a few of the GML standard and target air tanks, we dropped early calibration results that would bias the best fit derivation and assignment during the time of use of the tank.

### 2.3.2 Comparison of measurements of gas mixtures in cylinders with MPI-BGC

Since 2016, the MPI-BGC GasLab has organized same tank air measurement ("MENI") comparisons between WMO GAW partner laboratories as part of the European ICOS (Integrated Carbon Observation System) Flask and Calibration Laboratory quality control work. In this program, three 10L aluminum cylinders (Luxfer UK) are filled with dry air and maintained by the MPI-BGC and sent to measurement laboratories in a round robin loop. Two of the three cylinders had the same air mixture and showed small growth in their $H_2$ mole fractions over time. The third cylinder contains an "unknown" new mixture for each round robin loop.

Between 2016 and 2021, the MENI cylinders came to GML three times and were analyzed two to four times on the H9 instrument during each round robin stop. Some results were rejected due to poor instrument performance or the use of an alternate calibration strategy than the one used to transfer the scale. For the blind and ambient $H_2$ MENI cylinders the retained NOAA $H_2$ results agree well with the MPI_BGC measurements (< 1 ppb difference, SI Figure 5 a,b). For the low $H_2$ cylinder, the 2017/2018 NOAA measurements are biased low by about 2 ppb while the March 10, 2021 result is about 2 ppb

higher (SI Figure 5c). The MENI program provides a valuable on-going check for the MPI X2009 $H_2$ calibration scale transfer in GML.

### 2.3.3 Flask analysis systems target air tanks

Figure 5a shows the calibration histories on H9 for target air tanks used in the flask analysis laboratory between 2009 and 2022. $H_2$ increased in all the target tanks, sometimes rapidly, requiring time dependent value assignments.

Three $H_2$ target air tanks were in service between 2009 and 2019 and have been used to evaluate the GML calibration scale transfer to the MAGICC-1 and MAGICC-2 $H_2$ measurements (CC1824, CB08834 and CC303036). These tanks, however, exhibited rapid and large drifts and were not measured on H9 on a regular basis making it more difficult to use them to evaluate potential biases on MAGICC-1 and MAGICC-2 over this time period.

The target air tanks ALMX067998 and CB11143 entered service in 2016 and 2019 respectively with more frequent measurements on the calibration system to better define their time dependent value assignments. A new set of six target air tanks were prepared at the Niwot Ridge facility in late 2019 for the MAGICC-3 system. They have been analyzed on MAGICC-3 multiple times a year but only one of them has a $H_2$ mole fraction that remained below 700 ppb: CB10292.

With the caveats that the non-linear drift in aluminum cylinders may not be well modeled by a simple quadratic polynomial and that many of the early target tanks were under calibrated, the best polynomial fit to the calibration records for all target air tanks give residuals smaller than 1.2 ppb (Figure 5b). Details for the target tanks, including the best fit coefficients and the standard deviation of residuals to the fits are in SI Table 5.

In Figure 6, we show the differences between the target tank analysis results on H8 and H11 and their time-dependent $H_2$ assignments (based on the best fit to their calibration histories on H9 discussed above). The differences are all within 4 ppb, however there are times when there are persistent biases between the flask analysis system(s) and the calibration system. Uncertainties on the value assignment of the target air tanks, the value assignments and stability of the standards used to calibrate the flask analysis systems as well as the noise in the H8 and H11 measurements all contribute to the observed differences. Similar offsets on both flask analysis systems (for example CC1824 prior to 2012) may point to the main uncertainty contribution being from the value assignment of the target air tank. Different patterns in the offsets between the two flask analysis systems (for example offsets of different signs for CC303036 and CB08834 on H8 and H11 in 2011-2013) suggest the offsets are due to value assignments of the flask analysis system standards. Again, this is often due to limited calibration histories not being able to fully map the non-linear drift in the standards. It also indicates there are times with systematic differences (mostly < 2ppb) between the MAGGIC-1/H11 and MAGICC-2/H8 measurements in the flask records.

The full transition to the new MAGICC-3 system for flask analyses in August 2019 is indicated by the vertical bar in Figure 6. As discussed earlier, one improvement in this new system is that $H_2$ measurements are now calibrated using a multi-point calibration curve from a suite of standards. This

makes the measurement results less sensitive to drift or value assignment error in any individual standard since we are fitting multiple standards. We also now appreciate the complex $H_2$ growth patterns that can occur in aluminum cylinders so have undertaken regular calibrations to ensure drift is tracked closely. These changes seem to have reduced the bias observed between the flask analysis system and the calibration system, which gives confidence that future measurements will be higher quality.

To help us monitor the $H_2$ calibration scale propagation performance going forward, a new target air tank in an Essex stainless steel cylinder, SX-1009237, was filled in late 2022 to augment the current target tanks. This target air tank should be stable for $H_2$ and will be used for periodic comparison between measurement systems. Analysis results on H9 and H11 in December 2022 are 526.75 and 527.15 ppb, respectively, consistent with the residuals for other target air tanks at that time.

## 3 NOAA flask air $H_2$ measurements

Close to 6000 flask air samples from the  Cooperative Global Air Sampling Network are analyzed in GML every year. The network sites are chosen carefully to be representative of large scale air masses and to be able to rely on local support for sampling and shipping logistics. The reprocessing and release of the 2009-2021 $H_2$ global network flask air measurements on the MPI X2009 scale was made possible because of continued efforts to conduct and improve the $H_2$ measurements, to store all the necessary data, and to develop and update the tools for reliable and traceable reprocessing, comparison, and archiving.

### 3.1 Data quality assurance and quality control

In this section, we first describe the flask sample collection protocol and introduce the data quality control tags used to document sample and measurement data quality issues. GML flask air $H_2$ measurements data quality is evaluated using results from the daily analysis of test air flask pairs and from the agreement between South Pole Observatory (SPO) flask pairs. Finally, we present a preliminary estimation for the uncertainty of flask air $H_2$ measurements over 2009-2021, that includes empirical uncertainty estimates for the standards' assignments and the short-term noise of the instruments.

#### 3.1.1 Flask air sample collection overview and data quality tagging

Partners in the NOAA Cooperative Global Air Sampling Network collect whole outside air samples in glass flasks in pairs, upwind from any local sources of pollution, people and animals and away from structures or terrain that would affect the wind flow. Two 2.5L glass flasks with two glass stopcocks with Teflon o-rings are connected in series in a portable sampling unit (PSU) made of a rugged case, a battery, a pump, an intake line, and a mechanism to control the pressure of the air samples. Most sampling units include a dryer and are semi-automated, with the exception of those used at relatively dry high latitude locations and a few other locations where a more rugged, manually operated sampling unit is required. At most sites, the operator will carry the equipment outdoors to conduct the sampling. At a few sites, the PSU is indoors and connected to a fixed inlet line drawing air from the outside.

Before flasks are shipped to sampling sites, the glass flasks are filled with synthetic air in the GML flask logistics laboratory. During the sample collection on site, the flasks are first flushed for several minutes

and then filled to a pressure of 4 to 5 psi above ambient pressure in about 1 minute (See video: https://gml.noaa.gov/education/intheair.html).

Air sample collection and/or measurement issues that are documented or detected and known to affect a sample quality or an analyte measurement result are recorded with data quality control tags in our internal database. For each flask air measurement, internal data quality control tags are translated into a simpler 3 column flag indicating if the measurement is retained or rejected for external data users. The GML flask air samples and measurements can also have informational tags and comments, for example if another measurement laboratory analyzed an air sample before it came to GML for analysis (see same air measurement comparisons in section 3.3).

The global network flasks are filled to target pressure of 17-20 psia, but the final fill pressure can vary by 3-4 psi, with some of the higher altitude sites having final pressures on the lower range typically. If an air sample pressure is too low for the $H_2$ GC instrument on the MAGICC system, the $H_2$ measurement result is tagged as "rejected" for low sample pressure. If $H_2$ measurements in paired flasks have a 5 ppb or larger difference, the results for the pair are tagged as rejected. If only one member of the pair had an obvious issue (leak, low flask air pressure), only the $H_2$ measurement for that member is tagged as rejected. Some issues are detected by the MAGICC performance control system and are tagged automatically. Other issues are tagged manually by scientists as part of regular data quality control checks. Scientists also verify the validity of the automatic tags. Members of the team routinely evaluate if follow-up actions are needed to fix a sample collection or measurement issue or reduce the chance of rejecting future sample results for the same issue.

Some sites can experience brief high-pollution episodes with the $H_2$ mole fractions in both members of a pair meeting the pair agreement criteria but also being outliers, i.e. outside of the expected long-term variability at the site [Novelli et al., 1999]. Gross $H_2$ outliers are typically "tagged" manually. A statistical filter is applied before each annual data release [Dlugokencky et al., 1994]. For each site, a smoothing curve fit calculation determines the time series mean behavior broken down in a long-term trend, a seasonal cycle, and shorter-term (hours to weeks) variations [Thoning et al., 1989; Tans et al., 1989a]. The code is available and a link is provided further down. The filter works iteratively to find and tag outlier $H_2$ measurements when their residuals to the smooth curve fit is larger than 3 to 4 times the time series residuals' standard deviation.

### 3.1.2 Test air flask analysis results

Besides the regular analysis of target cylinders, the MAGICC flask analysis system is also tested daily using flasks filled with "test air" (flasks with site code "TST"). We have four rotating high pressure aluminum cylinders for test air (AL47-104, AL47-108, AL47-113, AL47-145), filled at the Niwot Ridge standard preparation site. SI Figure 6 shows their calibration histories on H9 for different fills. $H_2$ is not stable in the "test air" cylinders and for some tank-fills, $H_2$ increased rapidly and grew beyond our calibration range upper limit of 700 ppb.

Every 2 to 3 weeks an even number of TST flasks (14-24) are filled from the same test air cylinder. On typical analysis days, the MAGICC flask air measurement sequence will start with the analysis of air from two TST flasks with the same fill date.

Global network flask air samples are analyzed at NOAA GML only during the daytime to ensure the system operator is overseeing the full analysis cycle and minimizing the time a flask valve is open for the analysis. This is meant to minimize the risk of losing or contaminating the air samples as many of them are subsequently sent to the University of Colorado Boulder Stable Isotopes Laboratory for $CO_2$ and $CH_4$ isotope analyses.

Results from the TST flask pairs with the same fill date and analyzed on successive days give an indication of the short-term repeatability of the measurements. Here, the deviations from the mean $H_2$ in TST flasks with the same fill date are evaluated. For fill dates with a mean $H_2$ mole fraction less than 700 ppb, we calculate the differences between individual TST flask $H_2$ and the fill date mean. The standard deviation of the TST flasks $H_2$ differences from their fill date mean is 1.39 ppb on MAGICC-2/H8 (N=872), 0.73 ppb on MAGICC-1/H11 (N=3583), 1.55 ppb on MAGICC-3/H8 (N=504) and 0.68 ppb on MAGICC-3/H11 (N=1085), reflecting the higher measurement noise on H8.

Another diagnostic is the comparison of the TST flasks $H_2$ results and their test air cylinders' time-dependent assignments for the dates the TST flasks were filled based on the best fit of the H9 test air tank calibration results. This analysis is limited to the test air with less than 700 ppb $H_2$ and with tank calibration results on H9 that reasonably capture the increase in $H_2$: AL47-108 (F), AL47-113 (D,E,G), AL47-145 (F,G), AL47-104 (I). In SI Figure 7 (a-c), we show the $H_2$ differences between the TST flask results and their test air cylinder assignments. The differences reflect noise in the flask air measurements and uncertainties (and potentially small biases) in the test air tank-fill assigned $H_2$.

Between 2010 and 2021, the three fills of test air cylinder AL47-113 are in the ambient range and have the most stable $H_2$ mole fractions. The tank-fill assigned $H_2$ linear drift rate is 1 ppb/yr in fill D, null in fill E and 0.4 ppb/yr in fill G. Table 3 shows the mean and standard deviation of the differences in $H_2$ between TST flasks and the assigned $H_2$ in a stable or slowly drifting test air tank-fill. The biases for these subsets of TST air data are less than 1 ppb and the standard deviation is equal to or less than 1.5 ppb and is smaller for the most recent MAGICC-3/H11 configuration, which has a smaller number of data points.

### 3.1.3 South Pole Observatory: $H_2$ differences in flask pairs

The South Pole Observatory (site code SPO, sampling location: 89.98°S, 24.80°W, 2810 meters above sea level (masl)) gives scientists access to some of the "cleanest" air on Earth due to its remote location, and thus provides an opportunity to use SPO flask data as a quality assurance tool.

Two flask pairs are typically collected weekly and close in time at the four NOAA atmospheric baseline observatories using two collection methods. In method 'S', flasks are filled inside a building by tapping the air continuously pumped for analysis on an in-situ GHG measurement system. Method, 'P' (or 'G') involves using a portable sampling unit with an inlet mast and pump set up outside the building, similarly to other global network sites.

Staff rotation and flask shipping to and from the South Pole Observatory happen during a limited time window during the Austral summer. While awaiting shipment, SPO flask air samples are stored in crates in a heated storage building. Every year, one large SPO flask shipment arrives in Boulder in December/January and another smaller shipment arrives in February/March. A year's worth of flasks is prepared and shipped to SPO during that same time window. Despite the longer storage for SPO flasks before analysis, we have not detected biases in $H_2$ measurements of those samples when compared with other high southern latitudes times series. SPO flask air $H_2$ measurements show close to a 20 ppb seasonal cycle and a ~15 ppb increase in the annual mean levels between 2010 and 2021 (Figure 7).

There is very little short-term variability in the surface air over Antarctica for long-lived GHGs, CO and $H_2$. The differences in the $H_2$ mole fractions in SPO paired samples therefore mostly reflect the short-term noise in the measurements. In SI Table 6 we report statistics for $H_2$ differences for the two flask sampling methods and the four measurement system configurations between 2009 and 2021 with H8 and H11. As observed for the TST flasks, measurements on H11 are less noisy than on H8, especially on the MAGICC-3 system. The average of the absolute differences for $H_2$ in SPO flask paired samples is less than 2 ppb ($\sigma \leq 1.3$ ppb) and methods S and P $H_2$ pair averages at SPO agree within 1 ppb on average ($\sigma \leq 1.7$ ppb).

### 3.1.4 Flask air $H_2$ uncertainty estimates

We have derived preliminary empirical uncertainty estimates for flask air $H_2$ measurements that fall in the 200-700 ppb range. For measurements on MAGICC-1 and MAGICC-2, the total uncertainty estimate comes from the combination of two uncertainties added in quadrature: 1) the uncertainty on the $H_2$ tertiary standard time-dependent assignment (SI Table 2) and 2) the instrument estimated repeatability (Table 4). If an offline assignment correction is applied to take into account changes in a standard drift rate toward the end of its use, the standard assignment uncertainty is increased. The H8 and H11 instrument repeatability estimates are listed in Table 4. For now, we assume a 0.5 ppb uncertainty on the MAGICC-3 instrument response calibrated with multiple standards. On-going work will allow us to refine this last uncertainty component estimate at a later date. Typical 1-sigma uncertainties for GML flask air $H_2$ measurements are 1.2 to 1.9 ppb on MAGICC-1, 1.4 to 2.8 ppb on MAGICC-2, 1.6 ppb on MAGICC-3/H8 and 0.8 ppb on MAGICC-3/H11.

## 3.2 Comparison with other GAW laboratories $H_2$ measurements

A small number of laboratories operate well-calibrated long-term measurements of important atmospheric trace gases. The WMO Global Atmospheric Watch (GAW) coordinates regular technical and scientific discussions with experts from these laboratories. Another important outcome of the WMO/GAW collaborations consists of routine comparisons to assess the data compatibility for measurements from different laboratories and programs [Francey et al., 1999; Masarie et al., 2001; Jordan and Steinberg, 2011; Worthy et al., 2023]. The WMO/GAW network compatibility goals for measurements of $H_2$ in well mixed background air is 2 ppb (see Table 1 in [WMO/GAW, 2020]). This means that for $H_2$, measurement records should not have persistent biases less than 2 ppb to be used in combination with other qualifying measurements in global budget, trend and large scale gradient analyses.

GML participates in several WMO GAW measurement comparison efforts. Same-flask air measurement comparisons consist of one member of a NOAA flask pair collected at a site being analyzed by a partner laboratory before being analyzed by GML. Co-located flask air measurement comparisons involve 2 or more measurement programs having samples collected at the same location and close in time. Historically, these and other "intercomparison" projects have been abbreviated ICPs, which we use in the text below. Here the GML flask air $H_2$ measurements data compatibility is assessed with results from on-going ICPs.

GML conducts same-flask air measurement comparisons at the Cape Grim Observatory (CGO, 40.68° S, 144.69° W,164 masl) with CSIRO, Australia and at the Ochsenkopf mountain top tower (OXK, 50.03° N, 11.81° E, 1085 masl) with MPI-BGC, Germany. Sampling at OXK was temporarily suspended between June 2019 and April 2021. The Alert/Dr Neil Trivett Observatory (ALT, 82.45° N -62.51° W, 190 masl) has facilitated the largest multi-laboratory flask air comparison experiment in the WMO GAW program [Worthy et al., 2023]. NOAA has colocated flask air samples from ALT with CSIRO and the MPI-BGC. The CSIRO and MPI-BGC $H_2$ measurements are also traceable to the MPI X2009 calibration scale.

In Table 5, we summarize the annual mean of the differences for $H_2$ measurements from different laboratory and flask combinations (same flask, same flask pair or colocated flasks) for CGO, OXK and ALT between 2010 and 2021. All measurements included in the comparisons are retained, meaning they have passed quality control checks.

Columns 2 and 3 show the annual means of the NOAA $H_2$ differences between the ICP flask and its pair mate at CGO and OXK. For CGO flask air samples collected before 2019, we find that the NOAA analysis for the NOAA ICP flask first measured at CSIRO often shows higher $H_2$ than in the non-ICP flask air sample. We suspect several of these ICP flasks had a small but detectable contamination for $H_2$. We have applied a rejection tag to NOAA analysis results for CGO ICP flasks with an $H_2$ mole fraction 2 ppb or more above $H_2$ in the non-ICP pair mate. This affected 165 ICP samples between 2009 and 2018 or 37% of all CGO ICP flasks collected between August 2009 and the end of 2021. For OXK, the NOAA analysis result for the ICP flask first measured at MPI-BGC often shows slightly higher $H_2$ than in the non-ICP flask (Table 5, 3rd column), and the annual mean bias is less than 1 ppb for all years.

The last 4 columns in Table 5 show interlaboratory $H_2$ measurement comparisons for CGO, OXK and ALT flask air samples. The annual mean differences are consistently less than 1.6 ppb for CGO and less than 2 ppb for OXK for 9 out of 11 years (Figure 8). For colocated air samples at ALT we compare the mean of flask results for each laboratory and limit the comparison for samples collected within 60 minutes of each other. The ALT annual mean differences vary from year to year, and are less than +/- 2 ppb for 8 years out of 12 for the NOAA vs CSIRO comparison and for 7 years out of 10 for the NOAA vs MPI-BGC comparison. These on-going ICPs are monitored regularly to continually assess the NOAA $H_2$ data compatibility with data from GAW partners.

## 4. NOAA atmospheric $H_2$ time series

Previous measurement studies have described the $H_2$ global distribution for different time periods [Khalil

and Rasmussen, 1990; Novelli et al., 1999; Langenfelds et al., 2002; Price et al., 2007; Yver et al., 2011]. Some of the spatiotemporal features in the more recent NOAA $H_2$ measurement records are described in this section.

### 4.1 $H_2$ at the NOAA Cooperative Global Air Sampling Network Sites

There are 51 sites considered active or recently terminated in the Cooperative Global Air Sampling Network (see map in SI Figure 8 and site information in SI Table 7). The $H_2$ measurement times series for these sites are shown in SI Figure 9. Note that a few sites that have been discontinued are not shown in this figure. A curve fit is run for each site time series based on Thoning et al. [1989]. First the code optimizes parameters for a function made of a four-term harmonic and a cubic polynomial. The resulting residuals (measurements minus function) are then smoothed with a low-pass filter with a 667-day cutoff and are added to the polynomial part of the function to produce the "trend curve" (shown as the dark blue line in SI Figure 9). The residuals are also smoothed with a low-pass filter with a 80 day cutoff and are added to the function to produce a "smooth curve" at each site.

The data quality control work on our long-term measurement time series includes a data selection step with a statistical filter (see section 3.1.1). Samples with $H_2$ beyond 3.5 (4 for Ascension Island, ASC) standard deviations of the time series smoothed curve at each site are flagged as not representative of background air conditions and are shown as crosses in SI Figure 9.

The annual mean, maximum and minimum $H_2$ values of the smooth curve for the 51 sites are plotted in Figure 9 (in order of decreasing latitude along the x-axis) for years with retained measurements up to 2021. Sampling at the TPI site, on Taiping Island, Taiwan, started in May 2019, which explains the 2 (full sampling year) data points for the site. Sampling at a few network sites was impacted by the COVID-19 pandemic resulting in data gaps or delayed return shipping of samples. We recommend data users become familiar with individual sampling site measurement records to best aggregate and interpret signals.

The interhemispheric gradient of $H_2$, with higher levels in the SH, is apparent in the annual means distribution across sites (Figure 9, green circles). The majority of sites in the SH (BKT to SPO on the right side of Figure 9) show smaller seasonal cycle amplitudes (<23 ppb) than NH sites; however, several sites have interannual variations in their $H_2$ seasonal cycle amplitudes (SI Figure 9). Sites with the lowest $H_2$ seasonal minima (Figure 9, blue x symbols) likely are the most influenced by soil uptake. A few sites (for ex. TAP (Taiwan), AMY (Republic of Korea), LLN (Taiwan), CPT (South Africa)) show higher smooth curve annual maxima (Figure 9, red crosses), likely reflecting upwind local or regional emissions.

### 4.2 $H_2$ at NOAA Baseline Atmospheric Observatories

NOAA GML operates four staffed atmospheric baseline observatories (https://gml.noaa.gov/obop/). The South Pole Observatory in Antarctica and the Mauna Loa (MLO, Hawaii) observatories were built in

connection with the 1957-1958 International Geophysical Year, a global effort bringing together 67 nations to study the Earth and in connection with the first launches of artificial satellites in Earth's orbit by the USA and the former Soviet Union. The South Pole Observatory in Antarctica was established with support from the US National Science Foundation and NOAA. The other two observatories near Utqiaġvik, formerly Barrow, (BRW) and Samoa (SMO) were established in 1973 and 1974 respectively.

All four NOAA atmospheric baseline observatories have an upwind clean air sector with no local sources of pollution. Every week, scientists on location collect discrete air samples preferentially when the near surface wind comes from the clean air sector. Figure 10 shows the reprocessed $H_2$ time series for the Observatories between 2009 and 2021. Valid "S" and "P" method flask air $H_2$ measurements are retained for the South Pole Observatory only. The "S" method flasks show contaminated $H_2$ at Samoa and show seasonal contamination at Utqiaġvik (Barrow) until August 2021 when sampling started at a new tower with new sampling lines. The Mauna Loa $H_2$ in "S" method flasks will be further evaluated and may be retained in future releases.

The Samoa and South Pole $H_2$ smooth curves show similar maximum levels between 550 and 570 ppb and slightly higher minima at Samoa compared to the South Pole. The seasonal maximum occurs about 3 months earlier at Samoa than at the South Pole. The interannual variability is similar at both sites and is dominated by step increases on three occasions: in 2012/2013, 2016 and 2020.

The Mauna Loa $H_2$ time series shows more short-term variability than for Samoa and South Pole. The seasonal cycle amplitude of the Mauna Loa $H_2$ smooth curve is about 40 ppb with maximum levels in April-May and minimum levels in December-January. The seasonal maximum ranges from 550 to 580 ppb and the seasonal minimum ranges from 505 to 520 ppb. The measurements indicate that annual mean $H_2$ levels at Mauna Loa after 2016 were higher than in previous years.

Of the four observatories, the Barrow $H_2$ time series shows the lowest levels and the strongest seasonal cycle, about 60 ppb on average. The smooth curve seasonal maximum ranges from 520 to 540 ppb in April-May and the seasonal minimum in September-November ranges from 450 to 490 ppb.

Despite having larger emissions in the NH, the $H_2$ interhemispheric gradient shows lower levels in the extratropical NH. This is related to the larger land masses in the NH and the soil sink being the dominant removal process for $H_2$. Warwick et al. [2022] report model-based estimates for the $H_2$ lifetime of 8.3 years for the OH sink (from the authors base model configuration) and of 2.5 years for the soil uptake (average of existing literature studies). In their flux inversion, Yver et al. [2011] estimated that the NH high latitudes and the tropics represent 40% and 55% of the global soil sink respectively. The soil sink and OH sink in extratropical northern latitudes both peak in summertime [Price et al., 2007] leading to the observed stronger $H_2$ minima.

It is important to look at data from multiple sites to study and detect interannual and potentially long-term large-scale changes in atmospheric $H_2$ levels. In the next section, we present background air zonal mean $H_2$ time series based on samples collected at marine boundary layer sites.

### 4.3 $H_2$ marine boundary layer global and zonal means

To extract large scale signals from the global air sampling network, we use the NOAA GML marine boundary layer (MBL) zonal data product [Tans et al., 1989b; Dlugokencky et al., 1994]. Time series from remote MBL sites are smoothed and interpolated to produce a latitude versus time surface of the $H_2$ mean MBL mole fraction (Figure 11). For $H_2$, the number of sites included in the zonal mean calculations ranges from 29-42 sites until July 2017 when sampling from the Pacific Ocean shipboard (POC) was stopped, after which 24-27 sites were included in the calculation. Because the Cooperative Global Air Sampling Network is sparse in the tropics and in the SH mid latitudes, the MBL product likely does not equally detect and reflect interannual variability in fluxes in these under-sampled regions, for example biomass burning emissions in Africa and South America.

To further isolate changes in background $H_2$ at different latitudes, we first calculate MBL global and zonal means (shown in SI Figure 10) and then derive anomalies by removing the 2010-2021 average year from the global and zonal mean time series. Figure 12 shows the MBL anomaly for $H_2$ (black lines) and CO (dashed blue lines) for the global mean and 5 zonal band means (NH and SH Polar (53-90$^o$), NH and SH Temperate (17.5-53$^o$) and Tropics (17.5$^o$S to 17.5$^o$N). The NOAA GML CO measurements are for the same air samples as the $H_2$ measurements [Pétron et al., 2023b]. Here, we derive the global and zonal means for CO using the 2009-2022 MBL CO measurements and the anomalies are based on the 2010-2021 smooth curve zonal mean results to be consistent with the $H_2$ data analysis.

CO is emitted during incomplete combustion and is a useful marker of biomass burning emissions. CO has a shorter atmospheric lifetime than $H_2$ which results in shorter-lived CO anomalies from pulse emissions. The data reduction for the anomaly analysis is slightly different from Langenfelds et al. [2002] investigation of $CO_2$, $CH_4$, $H_2$, and CO interannual variability in the CSIRO network 1992-1999 time records. The CSIRO authors employed the same [Thoning et al., 1989] data smoothing technique as we do but used the derivative of the trend curve to analyze correlations in interannual growth rate variations between species. The anomaly approach chosen here allows to retain the timing of abrupt changes in the measurement records.

Over 2010-2021, background air $H_2$ has increased at all latitudes (Figure 12). The global mean MBL $H_2$ shows a non-uniform increase over this time with a noticeable 10 ppb step increase in 2016. The global mean MBL $H_2$ was 20.2 ±0.2 ppb higher in 2021 compared to 2010 (Figure 12a).

The meridional gradient and zonal band mean plots (Figures 11 and 12) highlight the evolution of background air $H_2$ at different latitudes. Anomalies in the smooth curves are useful to point to time periods when several successive air samples at a site show similar deviations from the average seasonal cycle and multi-year trend.

The 2016 $H_2$ step increase is detected in the Tropics and SH. In the Tropics it coincides with a strong positive CO anomaly that started in November 2015, reached a peak amplitude of 15 ppb mid-January 2016 and ended in May 2016. The 2015/2016 $H_2$ anomaly is first detected at Bukit Kototabang, Indonesia (BKT) and later at Ascension Island (ASC), Cape Grim (CGO) and Crozet Island (CRZ). Some BKT air samples impacted by biomass burning emissions show enhancements of 100s ppb in CO and $H_2$ (SI Figure 11). The 2015 fire season in Indonesia was among the most intense on record as shown by remote

sensing products of fire counts, CO and aerosols. Field et al. [2016] found that burning activities to clear peatland for farming likely contributed to larger emissions than expected from dry conditions alone in 2015.

There is another step increase in the Polar SH zonal band in early 2020, also coinciding with a pulse anomaly in CO (Figure 12f) likely related to large wildfires in Australia in late 2019-early 2020. The Cape Grim (CGO) and Crozet Island (CRZ) smoothed curves show a large jump between the late 2019 minimum and early 2020 maximum when the CGO CO measurement seasonal minimum is also 10-12 ppb higher than in other years (SI Figure 11). van der Welde et al. [2021] estimate that the 2019-2020 fires in Australia emitted 80% more $CO_2$ than "normal" Australian annual fire and fossil fuel emissions combined.

In the NH extratropics bands, positive anomalies in $H_2$ in 2021 coincide with CO pulse anomalies. For the Polar (Temperate) NH zonal band, the CO anomaly lasts from mid-July (June) to December 2021 with a peak in September and an anomaly maximum amplitude of 37 ppb (19 ppb). Record high emissions of $CO_2$ and CO from boreal forest fires in Eurasia and North America in 2021 have been reported by Zheng et al. [2023].

Previously, Simmonds et al. [2005] and Grant et al. [2010] have reported on the observed variability in the Mace Head continuous $H_2$ measurement record and linked interannual variability in the baseline annual mean $H_2$ to larger fire emission events. More recently, Derwent et al. [2023] shared an updated analysis of the February 1994-September 2022 Mace Head in-situ $H_2$ measurements. The in situ record shows higher monthly mean baseline $H_2$ levels in recent years and the authors report an increase in monthly mean anomalies after December 2015 (slope of 2.4 +/- 0.5 ppb/yr). They postulate that a "missing" source of increasing intensity after 2010 may be behind the observed sustained increased $H_2$, which is markedly different from the 1998-1999 anomalies attributed to biomass burning. Derwent et al. [2023] explore potential candidates for the missing sources. However, in the absence of strong and quantitative direct evidence at this time, additional studies are needed to interpret the observed $H_2$ variability.

## 5. Conclusions

In this paper, we have described how NOAA GML has adopted the MPI X2009 $H_2$ calibration scale. The work was confined to measurements on GC-HePDD instruments. The GML $H_2$ primary standards in electropolished stainless steel cylinders have been calibrated once by the MPI-BGC CCL in Fall 2020. We have used the CCL assignments to propagate the scale to secondary and tertiary standards. $H_2$ increases in most air standards stored in aluminum cylinders. A curve fit was applied to each standard calibration history to determine a time-dependent $H_2$ assignment on MPI X2009. The secondary and tertiary standards $H_2$ assignments were then used to reprocess results for NOAA flask air $H_2$ measurements on MPI X2009. The NOAA Cooperative Global Air Sampling Network flask reprocessed $H_2$ measurements for 2009-2021 are publicly available [Pétron et al., 2023a]. For the period 2010-2021,

same air measurements with GAW partner laboratories have annual mean differences less than 2 ppb for the Cape Grim comparison with CSIRO and less than 3 ppb for the Ochsenkopf comparison with MPI BGC. Over 2010-2021, background air $H_2$ has increased at all latitudes. However, site time series and marine boundary layer $H_2$ zonal means show significant interannual variability. We find that some of strongest $H_2$ zonal mean anomalies coincide with CO anomalies and therefore were likely partly driven by large biomass burning events in Indonesia (2015), Australia (2019/2020), and boreal latitudes (2012 and 2021) [Field et al., 2016; Petetin et al., 2018; Zheng et al., 2023]. A full analysis of the NOAA Cooperative Global Air Sampling Network $H_2$ measurement records is beyond the scope of this paper. This dataset complements WMO/GAW partner laboratories $H_2$ measurements and it will be updated and extended routinely moving forward.

## Data and Code Availability

The NOAA global network flask air $H_2$ and CO time series are available at https://doi.org/10.15138/WP0W-EZ08.

We kindly request that users of the NOAA $H_2$ dataset cite:

Pétron, G., Crotwell, A., Crotwell, M., Kitzis, D., Madronich, M., Mefford, T., Moglia, E., Mund, J., Neff, D., Thoning, K., & Wolter, S. (2023). Atmospheric Hydrogen Dry Air Mole Fractions from the NOAA GML Carbon Cycle Cooperative Global Air Sampling Network, 2009-2021 [Data set]. NOAA GML CCGG Division. Version: 2023-05-25, https://doi.org/10.15138/WP0W-EZ08

The python class used to filter and smooth time series data is available and explained at: https://gml.noaa.gov/aftp/user/thoning/ccgcrv/ccgfilt.pdf and the method can be referenced as [Thoning et al., 1989].

## Supplement

The supplement for this article is available in a separate file.

## Author Contributions

GP and AC designed the scale revision work. GP, AC and JM implemented the scale revision. GP, AC, MC, MM, DN and JM contributed to the data quality control. GP and JP analyzed network site time series. AC designed, built and oversaw the $H_2$ calibration scale transfer and the flask air analysis system operations, working with Paul Novelli until he retired in 2017. TM and AC carried out tank calibrations. BH prepared the primary standards. DK was in charge of the whole air standards, reference, target and test air tanks preparation. MM and EM were responsible for the flask air analysis lab operations, working with Patricia Lang until her retirement in 2019. EM managed the flask logistics laboratory and flask metadata entries. DN with support from SW managed the NOAA Cooperative Global Air Sampling Network. DN managed sampling equipment for sites. JM manages the database and date releases. JM, KT and AC developed code and user interfaces for data processing, quality control and exploration. AJ

calibrated the NOAA primary standards. AJ, PK and RL contributed data from their measurement programs. GP prepared the manuscript with contributions from AC and AJ and edits from BH, MC, RL, and JP.

## Competing Interests

The authors declare that they have no conflict of interest.


## Acknowledgements

We are grateful for our partners worldwide who collect and ship flask air samples to NOAA GML, Boulder, CO, for analysis. We thank past and current NOAA GML and CU CIRES colleagues for their contributions to the network operations, measurements, data management and data quality control. Gary Morris and Kathryn McKain from GML, Simon O'Doherty and an anonymous referee provided valuable comments on the manuscript.

## Financial support

This work was supported in part by NOAA Cooperative Agreements NA17OAR4320101 and NA22OAR4320151 and by the U.S. Department of Energy's Office of Energy Efficiency and Renewable Energy (EERE) under the Hydrogen and Fuel Cell Technologies Office (HFTO). The views expressed herein do not necessarily represent the views of NOAA, the U.S. Department of Energy or the United States Government.

## References


Bertagni, M.B., Pacala, S.W., Paulot, F. et al. Risk of the hydrogen economy for atmospheric methane. Nat Commun 13, 7706, doi: 10.1038/s41467-022-35419-7, 2022.

Brito J., Wurm, F., Yáñez-Serrano, A. M., de Assunção, J. V., Godoy, J. M., and Artaxo, P., Vehicular Emission Ratios of VOCs in a Megacity Impacted by Extensive Ethanol Use: Results of Ambient Measurements in São Paulo, Brazil, Environmental Science & Technology, 49 (19), 11381-11387, doi: 10.1021/acs.est.5b03281, 2015.

Ciais P., Tans, P. P., Trolier, M., et al., A Large Northern Hemisphere Terrestrial $CO_2$ Sink Indicated by the $^{13}C/^{12}C$ Ratio of Atmospheric $CO_2$. Science 269,1098-1102, doi: 10.1126/science.269.5227.1098, 1995.

Conway, T. J., Tans, P. P., Waterman, L. S., Thoning, K. W., Kitzis, D. R., Masarie, K. A., and Zhang, N., Evidence for interannual variability of the carbon cycle from the National Oceanic and Atmospheric Administration/Climate Monitoring and Diagnostics Laboratory Global Air Sampling Network, J. Geophys. Res., 99(D11), 22831–22855, doi:10.1029/94JD01951, 1994.

Cooper O.R., Schultz M. G., Schröder S., et al.; Multi-decadal surface ozone trends at globally distributed remote locations. Elementa: Science of the Anthropocene; doi:10.1525/elementa.420, 2020.

de Kleijne, K., de Coninck H., van Zelm, R., Huijbregts M. A., and V. Hanssen S. V., The many greenhouse gas footprints of green hydrogen, Sustainable Energy Fuels, 6, 4383-4387, doi: 10.1039/D2SE00444E, 2022.

Derwent, R. G., Simmonds, P. G., O'Doherty, S., Manning, A. J., Spain, T. G., High-frequency, continuous hydrogen observations at Mace Head, Ireland from 1994 to 2022: Baselines, pollution events and 'missing' sources, Atmospheric Environment, Volume 312, doi: 10.1016/j.atmosenv.2023.120029, 2023.

Dlugokencky, E. J., Steele, L. P., Lang, P. M., and Masarie, K. A., The growth rate and distribution of atmospheric methane, *J. Geophys. Res.*, 99( D8), 17021– 17043, doi:10.1029/94JD01245, 1994.

Dlugokencky, E. J., Bruhwiler, L., White, J. W. C., et al., Observational constraints on recent increases in the atmospheric $CH_4$ burden, Geophys. Res. Lett., 36, L18803, doi:10.1029/2009GL039780, 2009.

Field, R. D., van der Werf, G. R., Fanin, T., et al., Indonesian fire activity and smoke pollution in 2015 show persistent nonlinear sensitivity to El Niño-induced drought. Proceedings of the National Academy of Sciences 113, 33(2016), 9204–9209, doi: 10.1073/pnas.1524888113, 2016.

Francey, R. J.; Steele, L. P. ;Langenfelds, R. L.; and B.C. Pak, High Precision Long-Term Monitoring of Radiatively Active and Related Trace Gases at Surface Sites and from Aircraft in the Southern Hemisphere Atmosphere, Journal of Atmospheric Sciences, pp. 279-285, https://doi.org/10.1175/1520-0469(1999)056%3C0279:HPLTMO%3E2.0.CO;2, 1999.

Francey, R. J.; Steele, L. P.; Spencer, D. A.; Langenfelds, R. L.; Law, R. M.; Krummel, P. B.; Fraser, P. J.; Etheridge, D. M.; Derek, N.; Coram, S. A.; Cooper, L. N.; Allison, C. E.; Porter, L.; Baly, S. The CSIRO (Australia) measurement of greenhouse gases in the global atmosphere. In: Report of the eleventh WMO/IAEA Meeting of Experts on Carbon Dioxide Concentration and Related Tracer Measurement Techniques; 2001; Tokyo, Japan. World Meteorological Organization; pp. 97-106. http://hdl.handle.net/102.100.100/194315, 2003. Last accessed December 29, 2023.

Friedlingstein, P., et al., Global Carbon Budget 2022, Earth Syst. Sci. Data, 14, 4811–4900, https://doi.org/10.5194/essd-14-4811-2022, 2022.

Grant, A., Witham, C. S., Simmonds, P. G., Manning, A. J., and O'Doherty, S.: A 15 year record of high-frequency, in situ measurements of hydrogen at Mace Head, Ireland, Atmos. Chem. Phys., 10, 1203–1214, doi: 10.5194/acp-10-1203-2010, 2010.

Heiskanen, J. et al., The Integrated Carbon Observation System in Europe. Bulletin of the American Meteorological Society 103 (3), pp. E855 - E872, doi: 10.1175/BAMS-D-19-0364.1, 2022.

Hydrogen Council and McKinsey & Company, Hydrogen Insights 2023, 23pp. Accessible at: https://hydrogencouncil.com/wp-content/uploads/2023/12/Hydrogen-Insights-Dec-2023-Update.pdf, 2023. Last accessed December 29, 2023.

International Energy Agency, Global Hydrogen Review 2022, IEA, Paris, https://www.iea.org/reports/global-hydrogen-review-2022, License: CC BY 4.0, 284pp, 2022. Last accessed December 29, 2023.

Jordan, A. and Steinberg, B.: Calibration of atmospheric hydrogen measurements, Atmos. Meas. Tech., 4, 509–521, doi: 10.5194/amt-4-509-2011, 2011.

Khalil, M. A. K., and Rasmussen, R. A., Seasonal cycles of hydrogen and carbon monoxide in the polar regions: Opposite phase relationships, Ant. J. U. S. , 23(5), 177-178, 1989.

Khalil, M. A. K. and Rasmussen, R. A., Global increase of atmospheric molecular hydrogen. Nature 347, 743–745, doi: 10.1038/347743a0, 1990.

Kitzis, D., Preparation and Stability of Standard Reference Air Mixtures, 2017. https://gml.noaa.gov/ccl/airstandard.html. Last accessed May 17, 2023.

Komhyr, W. D., R. H. Gammon, T. B. Harris, L. S. Waterman, T. J. Conway, W. R. Taylor, and K. W. Thoning, Global atmospheric $CO_2$ distribution and variations from 1968–1982 NOAA/GMCC $CO_2$ flask sample data, J. Geophys. Res., 90(D3), 5567–5596, doi:10.1029/JD090iD03p05567, 1985.

Langenfelds, R. L., Francey, R. J., Pak, B. C., Steele, L. P., Lloyd, J., Trudinger, C. M., and Allison, C. E., Interannual growth rate variations of atmospheric $CO_2$ and its $\delta^{13}C$, $H_2$, $CH_4$, and CO between 1992 and 1999 linked to biomass burning, Global Biogeochem. Cycles, 16(3), 1048, doi:10.1029/2001GB001466, 2002.

Longden T., Beck, F. J., Jotzo, F., Andrews, R., Prasad, M.,'Clean' hydrogen? – Comparing the emissions and costs of fossil fuel versus renewable electricity based hydrogen, Applied Energy, Volume 306, Part B, 118145, ISSN 0306-2619, doi: 10.1016/j.apenergy.2021.118145, 2022.

Masarie, K. A., Langenfelds, R. L., Allison, C.E., et al., NOAA/CSIRO Flask Air Intercomparison Experiment: A strategy for directly assessing consistency among atmospheric measurements made by independent laboratories, J. Geophys. Res., 106(D17), 20445–20464, doi:10.1029/2000JD000023, 2001.

Montzka, S.A., Dutton, G.S., Yu, P. et al. An unexpected and persistent increase in global emissions of ozone-depleting CFC-11. Nature 557, 413–417, doi: 10.1038/s41586-018-0106-2, 2018.

Novelli, P. C., Elkins, J.W., Steele, L. P., The Development and Evaluation of a Gravimetric Reference Scale For Measurements of Atmospheric Carbon Monoxide, J. Geophys. Res., 96, 13,109-13,121, doi: 10.1029/91JD01108, 1991.

Novelli, P. C., Steele, L. P., and Tans, P. P., Mixing ratios of carbon monoxide in the troposphere, J. Geophys. Res., 97, 20,731-20,750, doi:10.1029/92JD02010, 1992.

Novelli, P. C., Lang, P. M., Masarie, K. A., Hurst, D. F., Myers, R., and W., E. J.: Molecular hydrogen in the troposphere: Global distribution and budget, J. Geophys. Res., 104, 30427–30444, doi: 10.1029/1999JD900788, 1999.

Novelli, P. C., Crotwell, A. M., and Hall, B. D., Application of Gas Chromatography with a Pulsed Discharged Helium Ionization Detector for Measurements of Molecular Hydrogen, Env. Sci. Technol. (43), 2431-2436, doi: 10.1021/es803180g, 2009.

Ocko, I. B. and Hamburg, S. P.: Climate consequences of hydrogen emissions, Atmos. Chem. Phys., 22, 9349–9368, doi: 10.5194/acp-22-9349-2022, 2022.

Oltmans S. J. and Levy, H. II, Surface ozone measurements from a global network, Atmospheric Environment, Volume 28, Issue 1, Pages 9-24, ISSN 1352-2310, doi: 10.1016/1352-2310(94)90019-1, 1994.

Petetin, H., Sauvage, B., Parrington, M., Clark, H., Fontaine, A., Athier, G., Blot, R., Boulanger, D., Cousin, J.-M., Nédélec, P., and Thouret, V.: The role of biomass burning as derived from the

tropospheric CO vertical profiles measured by IAGOS aircraft in 2002–2017, Atmos. Chem. Phys., 18, 17277–17306, doi: 10.5194/acp-18-17277-2018, 2018.

Pétron, G., et al., Hydrocarbon emissions characterization in the Colorado Front Range: A pilot study, J. Geophys. Res., 117, D04304, doi:10.1029/2011JD016360, 2012.

Pétron, G., Crotwell, A., Crotwell, M., Kitzis, D., Madronich, M., Mefford, T., Moglia, E., Mund, J., Neff, D., Thoning, K., & Wolter, S., Atmospheric Hydrogen Dry Air Mole Fractions from the NOAA GML Carbon Cycle Cooperative Global Air Sampling Network, 2009-2021 [Data set]. NOAA GML CCGG Division. Version: 2023-05-25, doi: 10.15138/WP0W-EZ08, 2023a.

Pétron G., A.M. Crotwell, M.J. Crotwell, E. Dlugokencky, M. Madronich, E. Moglia, D. Neff, K. Thoning, S. Wolter, J.W. Mund, Atmospheric Carbon Monoxide Dry Air Mole Fractions from the NOAA GML Carbon Cycle Cooperative Global Air Sampling Network, 1988-2022, Version: 2023-08-28, doi: 10.15138/33bv-s284, 2023b.

Price, H., Jaegle, L., Rice, A., Quay, P., Novelli, P. C., and Gammon, R.: Global budget of molecular hydrogen and its deuterium content: Constraints from ground station, cruise, and aircraft observations, J. Geophy. Res., 112, D22108, doi:10.1029/2006JD008152, 2007.

Propper, R., Wong, P., Bui, S., Austin, J., Vance, W., Alvarado, Á., Croes, B., and Luo, D., Ambient and Emission Trends of Toxic Air Contaminants in California, Environmental Science & Technology, 49 (19), 11329-11339, doi: 10.1021/acs.est.5b02766, 2015.

Schultz, M.G., Akimoto, H., Bottenheim, J., et al., The Global Atmosphere Watch reactive gases measurement network. Elementa: Science of the Anthropocene, 3, doi: 10.12952/journal.elementa.000067, 2015.

Simmonds, P. G., Derwent, R. G., O'Doherty, S., Ryall, D. B., Steele, L. P., Langenfelds, R. L., Salameh, P., Wang, H. J., Dimmer, C. H., and Hudson, L. E.: Continuous high-frequency observations of hydrogen at the Mace Head baseline atmospheric monitoring station over the 1994–1998 period, J. Geophys. Res., 105, 12105–12121, doi: 10.1029/2000JD900007, 2000.

Simmonds, P. G., A.J. Manning, R.G. Derwent, P. Ciais, M. Ramonet, V. Kazan, D. Ryall, A burning question. Can recent growth rate anomalies in the greenhouse gases be attributed to large-scale biomass burning events?, Atmospheric Environment, Volume 39, Issue 14,Pages 2513-2517, doi: 10.1016/j.atmosenv.2005.02.018, 2005.

Simpson, I.J., M.P.S. Andersen, S. Meinardi, L. Bruhwiler, N.J. Blake, et al., Long-term decline of global atmospheric ethane concentrations and implications for methane. Nature, 488(7412):490–494, doi: 10.1038/nature11342, 2012.

Steele, L.P., Fraser, P.J., Rasmussen, R.A. et al. The global distribution of methane in the troposphere. J Atmos Chem 5, 125–171, doi: 10.1007/BF00048857, 1987.

Storm, I., Karstens, U., D'Onofrio, C., Vermeulen, A., and Peters, W.: A view of the European carbon flux landscape through the lens of the ICOS atmospheric observation network, Atmos. Chem. Phys., 23, 4993–5008, doi: 10.5194/acp-23-4993-2023, 2023.

Tans, P.P., Thoning, K.W., Elliot, W.P., and Conway, T.J., *Background atmospheric $CO_2$ patterns from weekly flask samples at Barrow, Alaska: Optimal signal recovery and error estimates,* NOAA Tech. Memo. (ERL-ARL-173). Environ. Res. Lab., Boulder, Colo., 131 pp. 1989a.

Tans, P.P., T.J. Conway, and T. Nakazawa, Latitudinal distribution of the sources and sinks of atmospheric carbon dioxide derived from surface observations and an atmospheric transport model, J. Geophys. Res., 94, 5151-5172, doi: 10.1029/JD094iD04p05151, 1989b.

Thompson A. M., J. C. Witte, S. J. Oltmans, F. J. Schmidlin, SHADOZ - A tropical ozonesonde-radiosonde network for the atmospheric community. Bulletin of the American Meteorological Society, Vol. 85, No. 10, pp. 1549-1564, http://www.jstor.org/stable/26221206, 2004.

Thoning, K.W., P.P. Tans, and W.D. Komhyr, Atmospheric carbon dioxide at Mauna Loa Observatory 2. Analysis of the NOAA GMCC data, 1974-1985, J. Geophys. Res., 94, 8549-8565, doi: 10.1029/JD094iD06p08549, 1989.

Tørseth, K., Aas, W., Breivik, K., Fjæraa, A. M., Fiebig, M., Hjellbrekke, A. G., Lund Myhre, C., Solberg, S., and Yttri, K. E.: Introduction to the European Monitoring and Evaluation Programme (EMEP) and observed atmospheric composition change during 1972–2009, Atmos. Chem. Phys., 12, 5447–5481, doi: 10.5194/acp-12-5447-2012, 2012.

van der Velde, I.R., van der Werf, G.R., Houweling, S. *et al.* Vast CO2 release from Australian fires in 2019–2020 constrained by satellite. *Nature* 597, 366–369, doi: 10.1038/s41586-021-03712-y, 2021.

von Schneidemesser E., Monks, P.S., Plass-Duelmer C., Global comparison of VOC and CO observations in urban areas, Atmospheric Environment, Volume 44, Issue 39,Pages 5053-5064, ISSN 1352-2310, doi: 10.1016/j.atmosenv.2010.09.010, 2010.

Yver, C. E., Pison, I. C., Fortems-Cheiney, A., A new estimation of the recent tropospheric molecular hydrogen budget using atmospheric observations and variational inversion, Atmos. Chem. Phys., 11, 3375–3392, doi: 10.5194/acp-11-3375-2011, 2011.

Warwick, N., Griffiths, P., Keeble, J., Archibald A., Pyle, J., and Shine, K.: Atmospheric implications of increased Hydrogen use, UK government's Department of Business, Energy and Industrial Strategy (BEIS) report, 2022. Accessible at: https://assets.publishing.service.gov.uk/media/624eca7fe90e0729f4400b99/atmospheric-implications-of-increased-hydrogen-use.pdf, Last accessed: October 18, 2023.

Warwick, N. J., Archibald, A. T., Griffiths, P. T., Keeble, J., O'Connor, F. M., Pyle, J. A., and Shine, K. P.: Atmospheric composition and climate impacts of a future hydrogen economy, Atmos. Chem. Phys., 23, 13451–13467, https://doi.org/10.5194/acp-23-13451-2023, 2023.

World Meteorological Organization, Global Atmospheric Watch, 20th WMO/IAEA Meeting on Carbon Dioxide, Other Greenhouse Gases and Related Measurement Techniques (GGMT-2019), report 255, 2020. Accessible at: https://library.wmo.int/records/item/57135-20th-wmo-iaea-meeting-on-carbon-dioxide-other-greenhouse-gases-and-related-measurement-techniques-ggmt-2019. Last accessed: December 4, 2023.

World Meteorological Organization, Greenhouse Gas Bulletin (18): The State of Greenhouse Gases in the Atmosphere Based on Global Observations through 2021. 10p., 2022. Accessible at: https://library.wmo.int/idurl/4/58743. Last accessed: January 2, 2024.

Worthy, D. E. J., Rauh, M. K., Huang, L., et al.,Results of a Long-Term International Comparison of Greenhouse Gas and Isotope Measurements at the Global Atmosphere Watch (GAW) Observatory in Alert, Nunavut, Canada, Atmos. Meas. Tech., 16, 5909–5935, doi: 10.5194/amt-16-5909-2023, 2023.

Yap, J., and McLellan B. A., Historical Analysis of Hydrogen Economy Research, Development, and Expectations, 1972 to 2020, Environments, *10*, 11, doi: 10.3390/environments10010011, 2023.

Zheng, B., Ciais, P., Chevallier, F., et al., Record-high $CO_2$ emissions from boreal fires in 2021. Science, 379, 912-917, doi: 10.1126/science.ade0805, 2023.

## Tables

Table 1. NOAA GML $H_2$ primary standards (prepared gravimetrically) and their WMO/MPI X2009 assignments (dated 2022-02-28). All $H_2$ dry air mole fractions and their uncertainties are in ppb.

| Serial Number | Fill code | Fill Date | CCL value | CCL uncertainty |
|---|---|---|---|---|
| SX-3558 | A | 2008-10-17 | 248.4 | 0.1 |
| SX-0614470 | A | 2019-04-15 | 352.8 | 0.1 |
| SX-3543 | B | 2008-11-03 | 425.4 | 0.2 |
| SX-3540 | B | 2007-08-07 | 488 | 0.2 |
| SX-0614471 | A | 2019-04-19 | 496.5 | 0.3 |
| SX-3523 | C | 2007-07-24 | 527 | 0.2 |
| SX-3554 | A | 2007-08-02 | 601.2 | 0.2 |
| SX-0614472 | A | 2019-04-19 | 701.9 | 0.2 |

Table 2: H9 Target air tanks with zero or linear growth in $H_2$

| Linear Drift Rate (ppb/yr) | Target Tank IDs | Standard deviation of residuals to best fits (ppb) |
|---|---|---|
| 0 | CA05278, CA06194, CA08247, CC121971, CC311842 ND16439, ND33960 | 0.46 |
| 0-1 | ALM-065166, CA05300, CC71607, CC73110 | 0.42 |
| 2-5 | CA04551, CA07328, CB10910 | 0.32 |
| 5-10 | CC71579 | 0.36 |
| > 20 | CA08145 | 0.48 |

Table 3. Summary statistics for $H_2$ differences between test air tank-fill assignment (based on H9 calibration history) and associated TST flask measurements on MAGICC systems

| System / Instrument | Test air tank id and fill | Differences mean (ppb) | Differences standard deviation (ppb) | Number of samples |
|---|---|---|---|---|
| MAGICC-2 / H8 | AL43-113 D, E | -0.3 | 1.3 | 528 |
| MAGICC-1 / H11 | AL43-113 D, E, G | +0.3 | 1.1 | 1231 |
| MAGICC-3 / H8 | AL47-145 G | -0.9 | 1.5 | 388 |
| MAGICC-3 / H11 | AL43-113 G | +0.4 | 0.6 | 144 |

Table 4: Flask air $H_2$ measurement uncertainty components

| Uncertainty components | 1 sigma uncertainty estimate (ppb) | Source |
|---|---|---|
| Tertiary standard time-dependent assignment uncertainty (1 point calibration) | 0.5-2.5<br>Tank specific (see SI Table 2) | Calibration histories, residuals to best fit, TST flasks |
| MAGICC-3 response curve uncertainty | 0.5 | Preliminary estimate, will be reassessed. |
| Measurement repeatability on H8 | 1.3 (MAGICC-2)<br>1.5 (MAGICC-3) | TST and SPO flask pair differences (Table 3 and SI Table 6) |
| Measurement repeatability on H11 | 1.1 (MAGICC-1)<br>0.6 (MAGICC-3) | |

Table 5: Annual mean of $H_2$ measurement differences (in ppb) for air samples from the Cape Grim Observatory (CGO), Ochsenkopf (OXK) and Alert (ALT). Non background air sample measurement results are included. Colocated (not same air) samples at ALT are matched within a +/- 60 minutes window.

| Year | NOAA ICP-NOAA nonICP | | CGO NOAA non ICP minus CSIRO ICP | OXK NOAA ICP minus MPI ICP | ALT NOAA minus CSIRO (not same air) | ALT NOAA minus MPI (not same air) |
|---|---|---|---|---|---|---|
| | CGO* | OXK | | | | |
| 2010 | - | -0.05 | 0.72 | -0.17 | -3.4 | -3.5 |
| 2011 | - | 0.15 | 0.50 | -0.02 | 2.2 | -3.9 |
| 2012 | 0.58 | 0.13 | 0.40 | -0.29 | 0.66 | -2.3 |
| 2013 | - | 0.01 | 0.23 | 0.80 | 1.30 | -1.4 |
| 2014 | - | 0.19 | 1.37 | 1.61 | 0.63 | -1.1 |
| 2015 | - | 0.85 | 0.02 | 0.53 | 0.52 | -1.4 |
| 2016 | 1.32 | 0.20 | 1.54 | 2.91 | -0.32 | -1.4 |
| 2017 | 1.19 | 0.56 | 1.38 | 2.49 | 3.2 | - |
| 2018 | 0.91 | 0.53 | 1.31 | 1.69 | 1.2 | -1.3 |
| 2019 | 0.73 | -0.07 | 0.30 | 1.25 | 1.0 | -0.81 |
| 2020 | 0.18 | na | 0.19 | - | 0.01 | -0.22 |
| 2021 | 0.33 | 0.33 | 0.86 | 1.71 | 3.4 | - |

*Most NOAA ICP flasks from CGO had a small contamination for CO and $H_2$ prior to 2019. If the NOAA ICP flask $H_2$ results are > 2ppb larger than the NOAA non-ICP flask $H_2$ in the pair, the ICP flask $H_2$ has been rejected. Only years with at least 10 valid $H_2$ pairs are included.

**Figures**

Figure 1. Calibration results for GML two $H_2$ secondary standards (a) CC119811 and b) CA03233 on H9 against one of the primary standards. 2019-2020 multipoint calibration results on H9 are also shown for CA03233 (pink circles). Only results shown with open circles are used for the assignments.

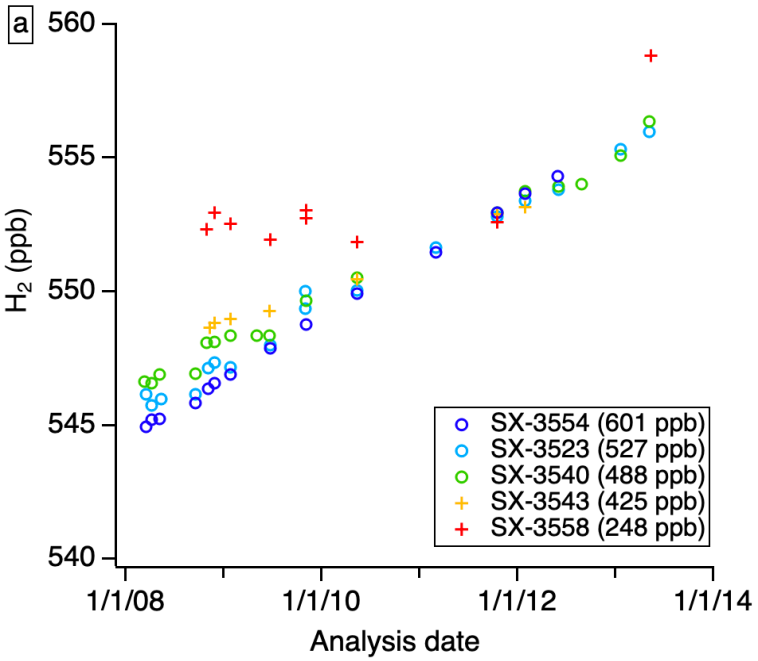


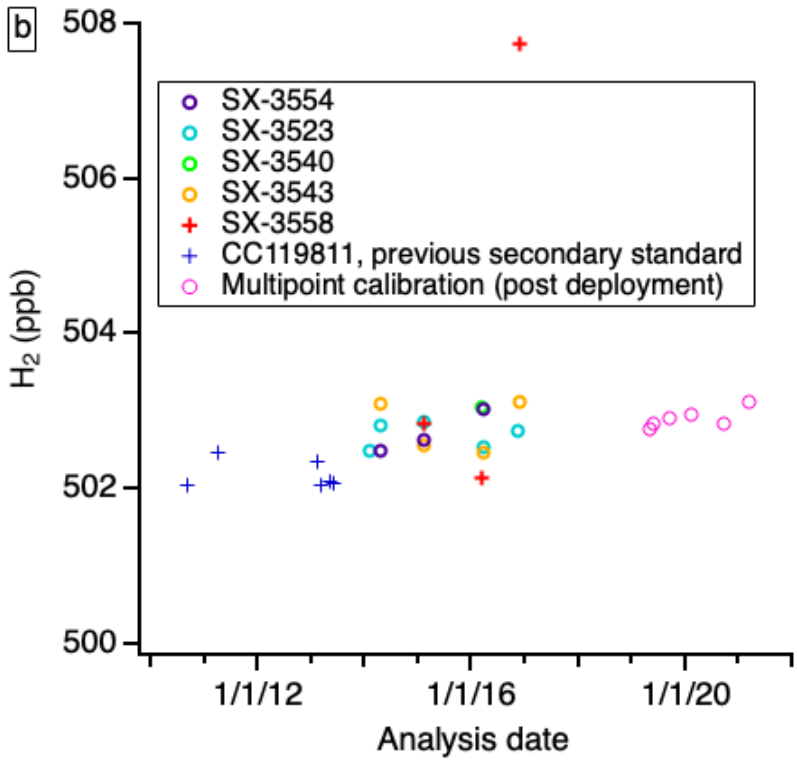

Figure 2: 2019-2022 H9 standard calibration response curve (RC) results: a) differences from the mean RC linear fit and b) residuals of the response curve fits. Different colors are for different calibration episodes.

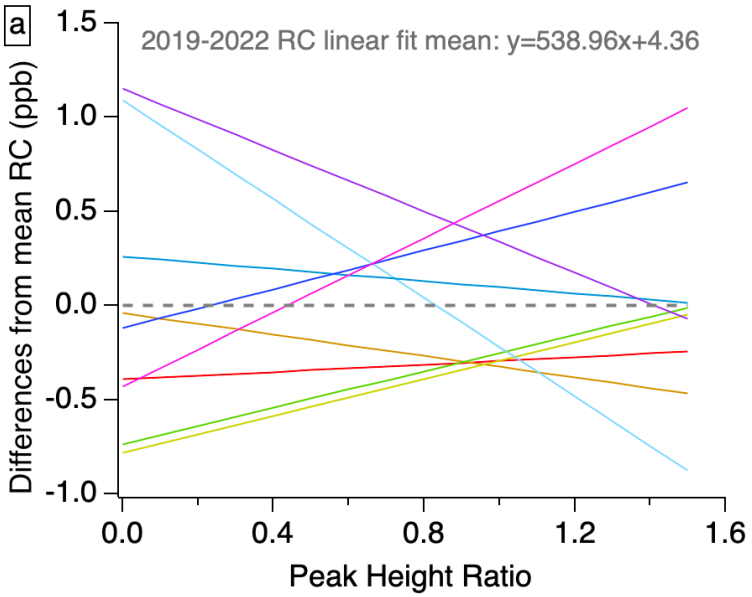


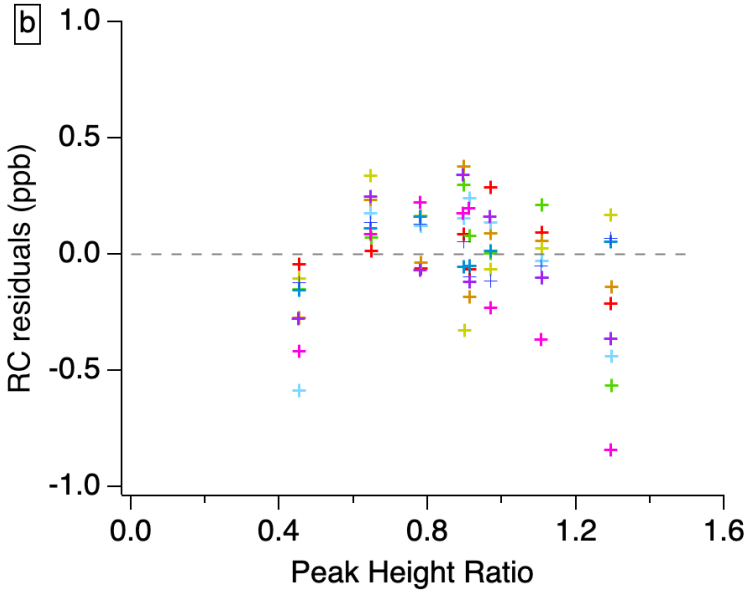

Figure 3. Calibration histories of a) MAGICC-1 / H11 and b) MAGICC-2 / H8 tertiary standards. The colored vertical line indicates when a standard started to be used.

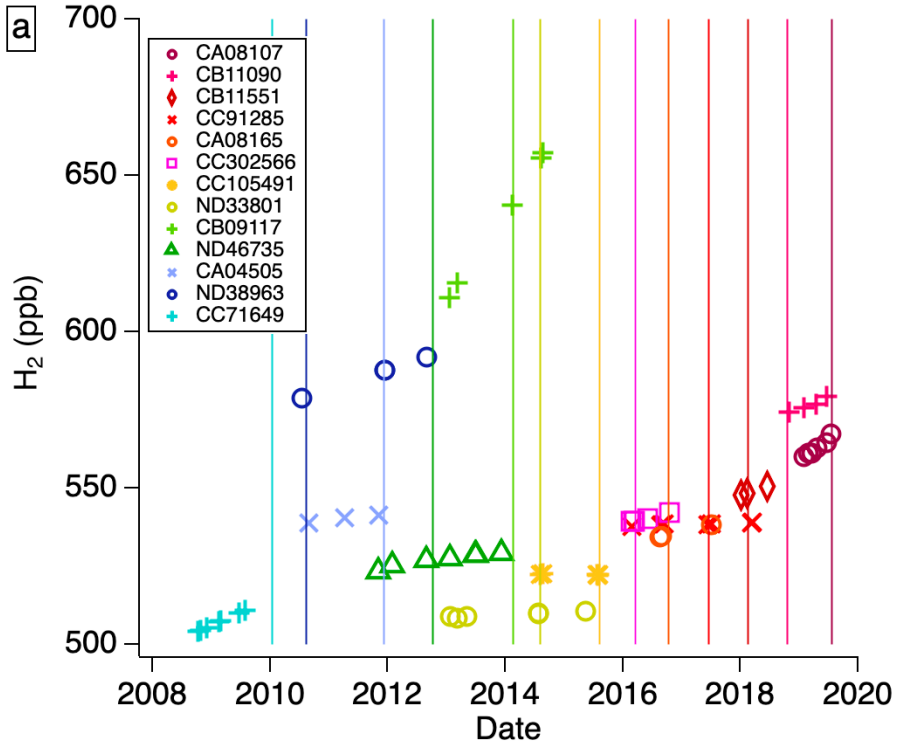


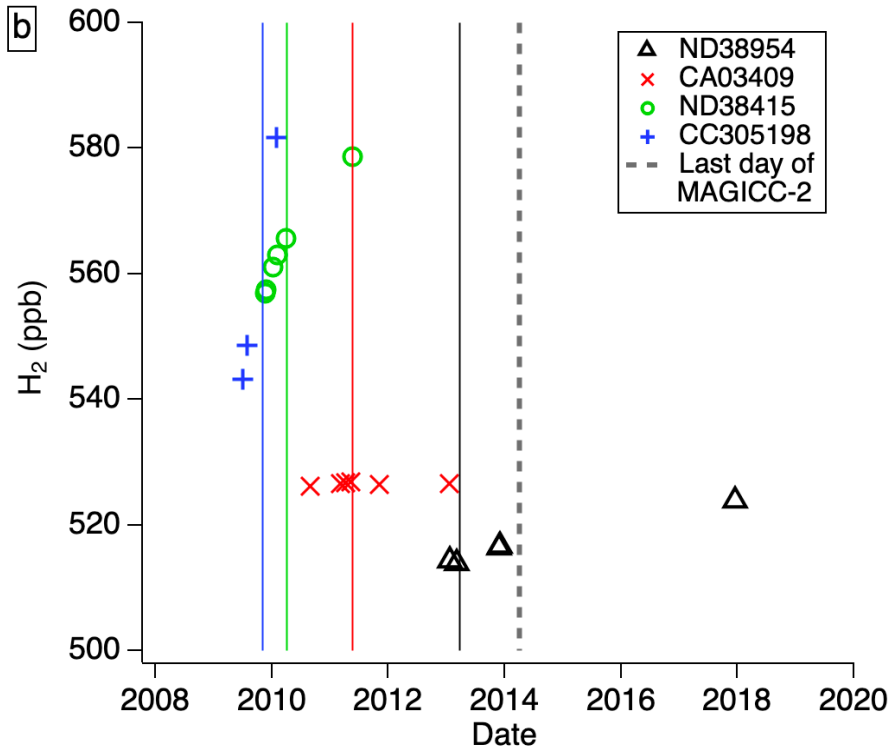

Figure 4: Calibration histories and residuals to best fit for H9 target tanks with a stable $H_2$ mole fraction or a linear drift less than 1 ppb/yr. Residuals are in ppb.

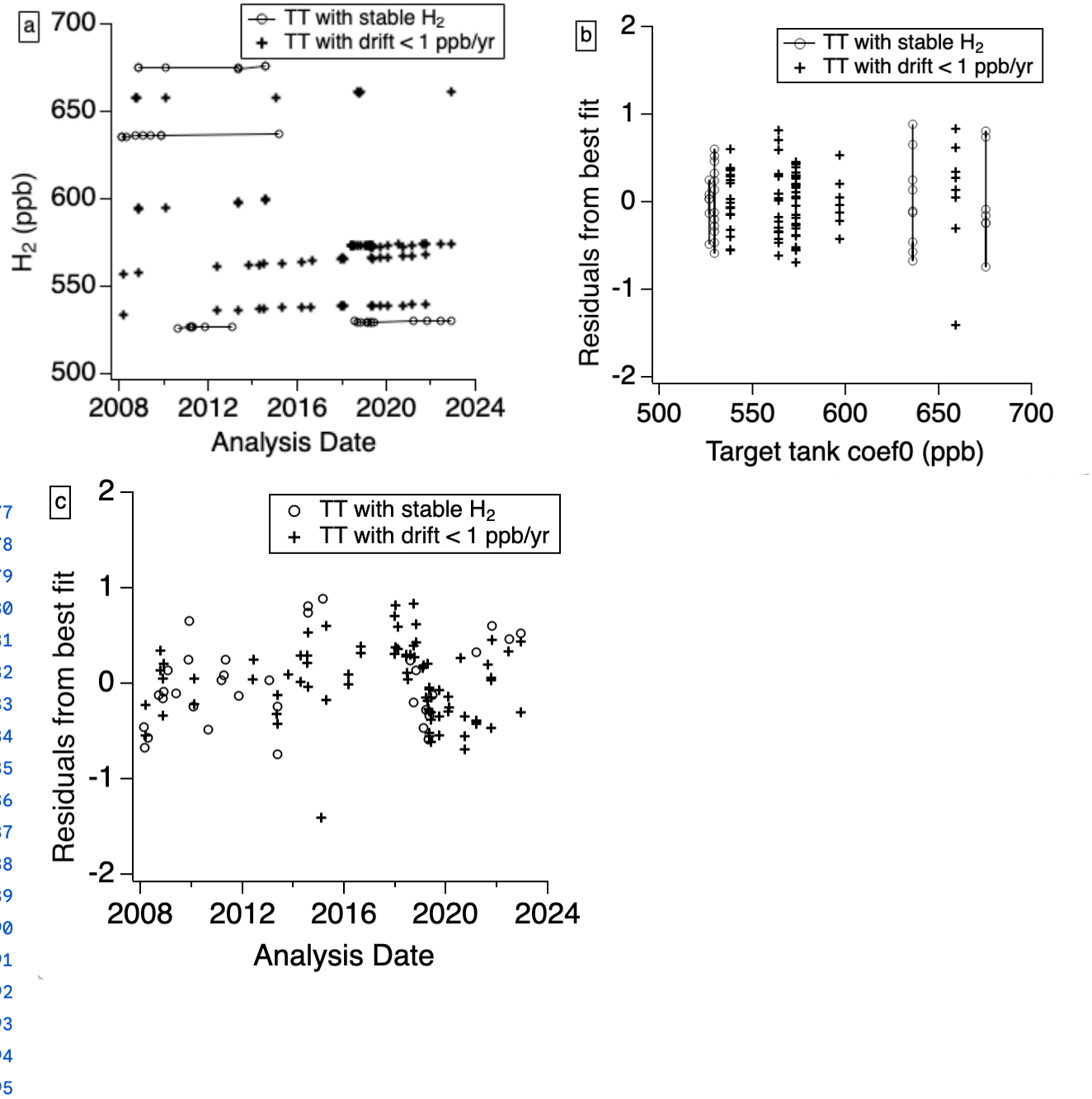

Figure 5. Flask air analysis systems target air tanks H9 a) calibration histories and b) residuals to best linear or quadratic fit.

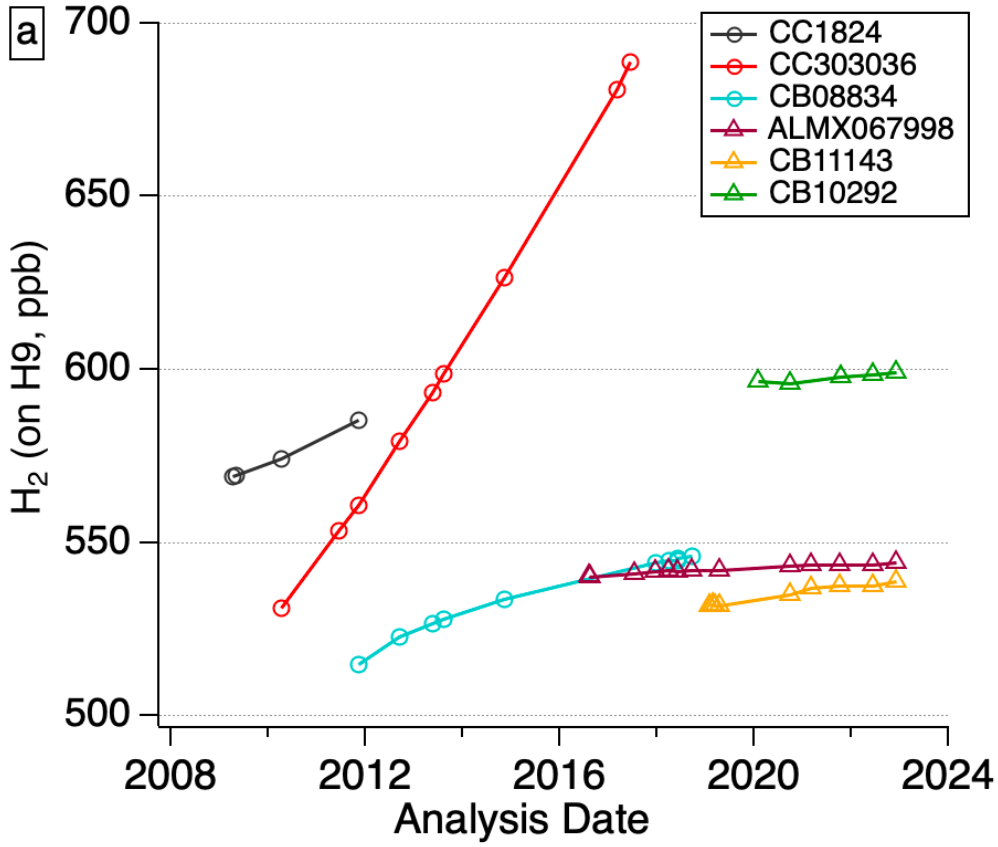

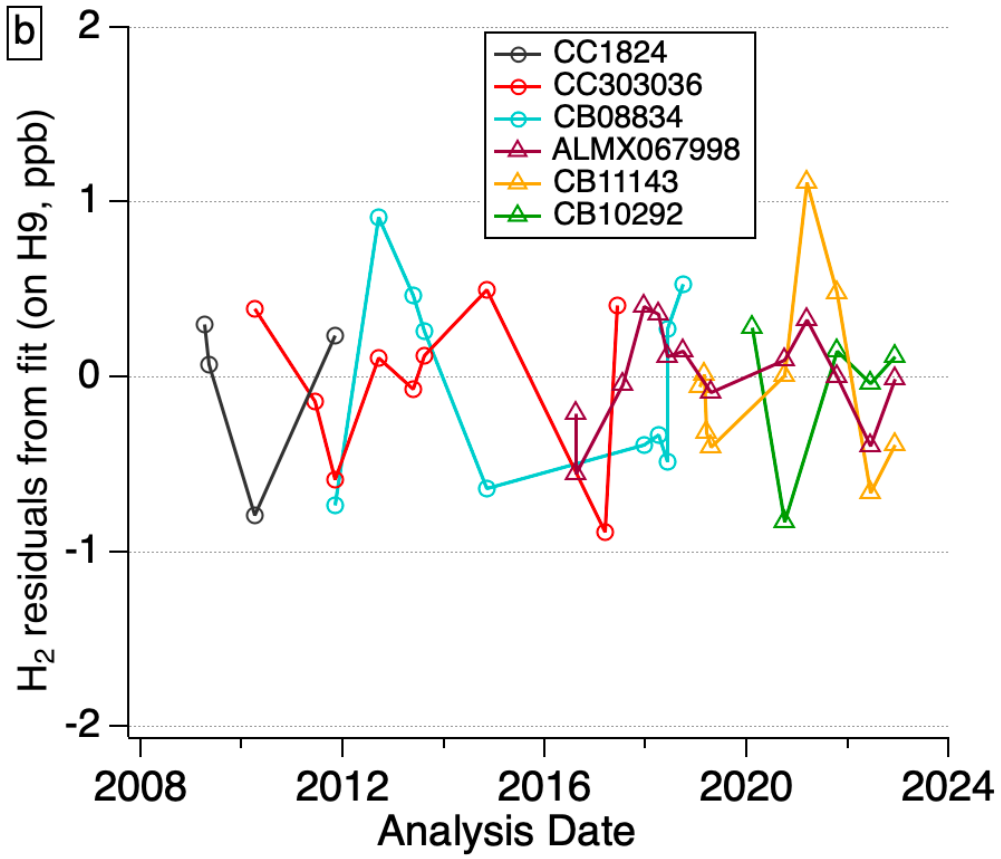
b
CC1824
CC303036
CB08834
ALMX067998
CB11143
CB10292
H2 residuals from fit (on H9, ppb)
2
1
0
-1
-2
2008
2012
2016
2020
2024
Analysis Date

Figure 6. Differences of target air tank $H_2$ analysis results on a) H11 and b) H8 and the time-dependent assignment based on calibration history on H9.

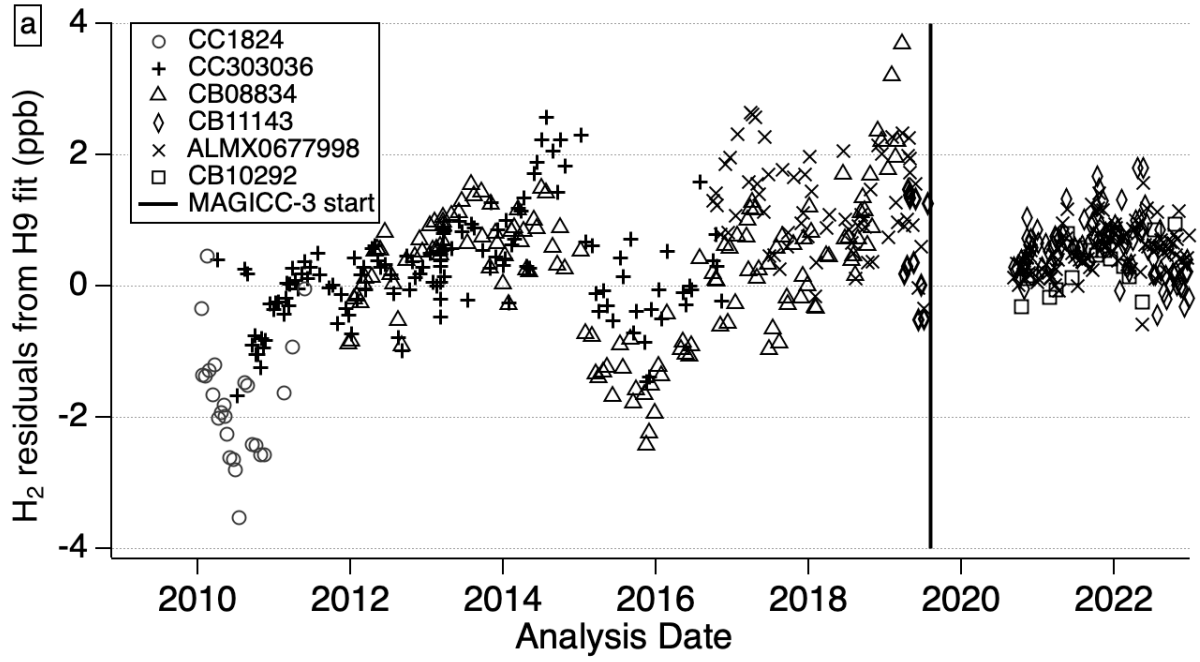


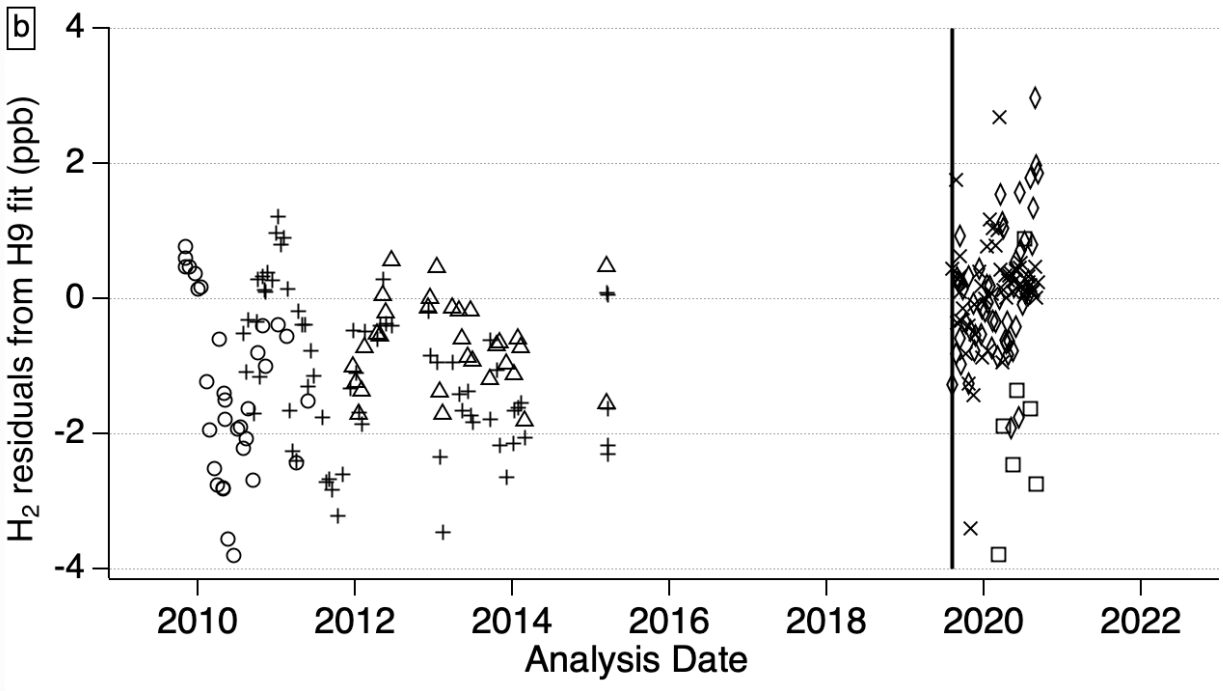

Figure 7. South Pole Observatory flask air $H_2$ measurements on H11 and H8. Black symbols are used for measurements of P flasks and blue symbols are used for measurements of S flasks.

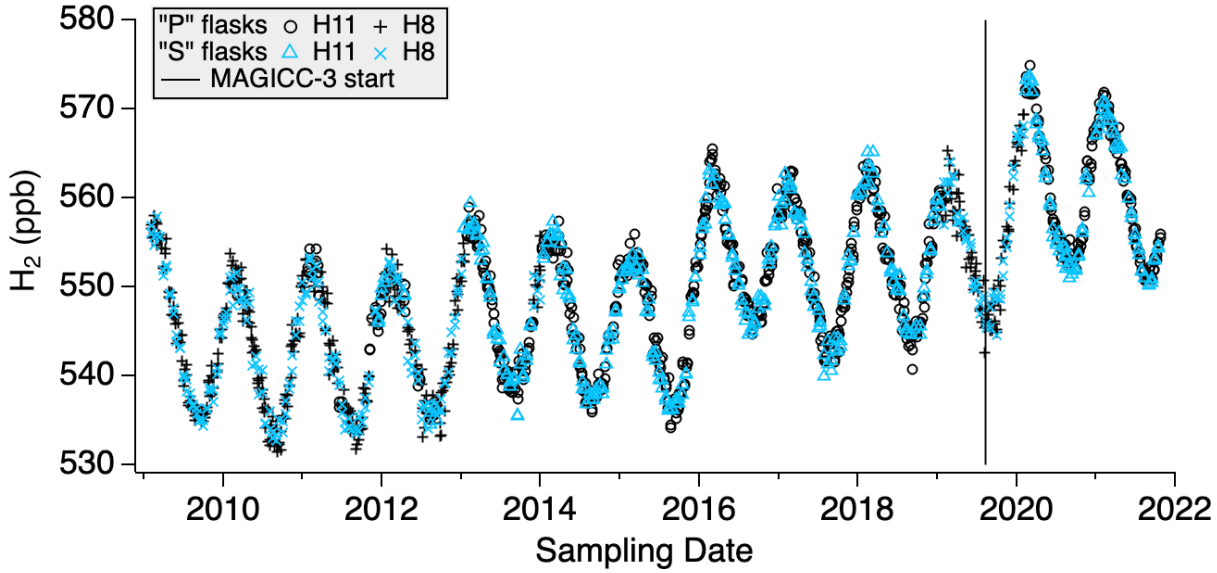


Figure 8. Interlaboratory same air $H_2$ measurement difference for OXK ICP (NOAA - MPI-BGC) and CGO (NOAA non ICP - CSIRO ICP).

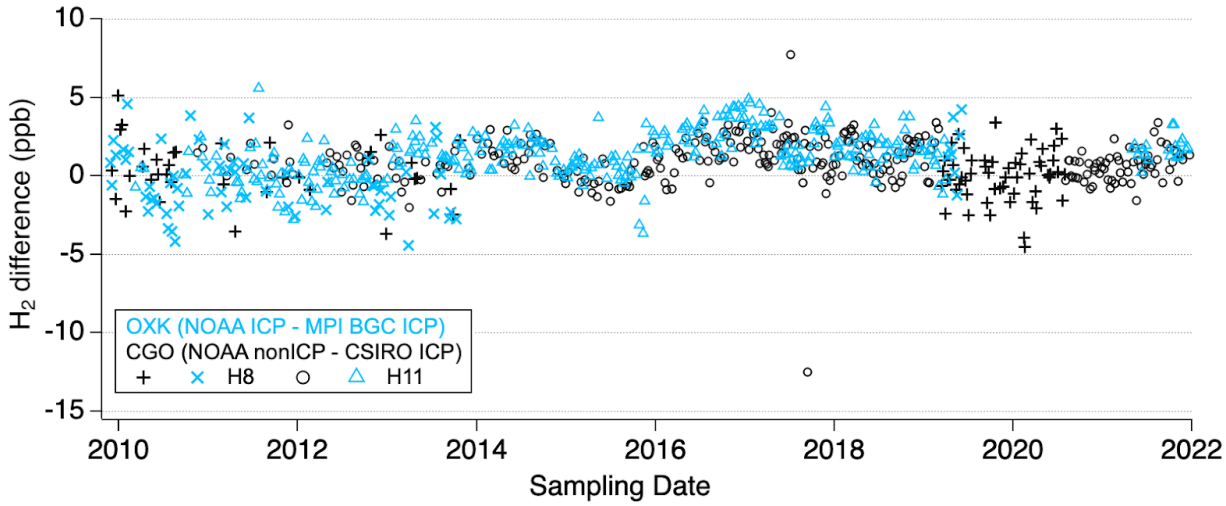


Figure 9: Annual maximum (red), mean (green) and minimum (blue) $H_2$ from the smooth curve fit of the 2010-2021 measurement time series for each surface site in the global sampling network. Each site is referred to with a three letter code (see details in SI Table 7). The sampling sites are shown along the x-axis with decreasing latitudes. An asterisk near the site code indicates if the site data are used for the marine boundary layer air zonal and global means $H_2$ data reduction.

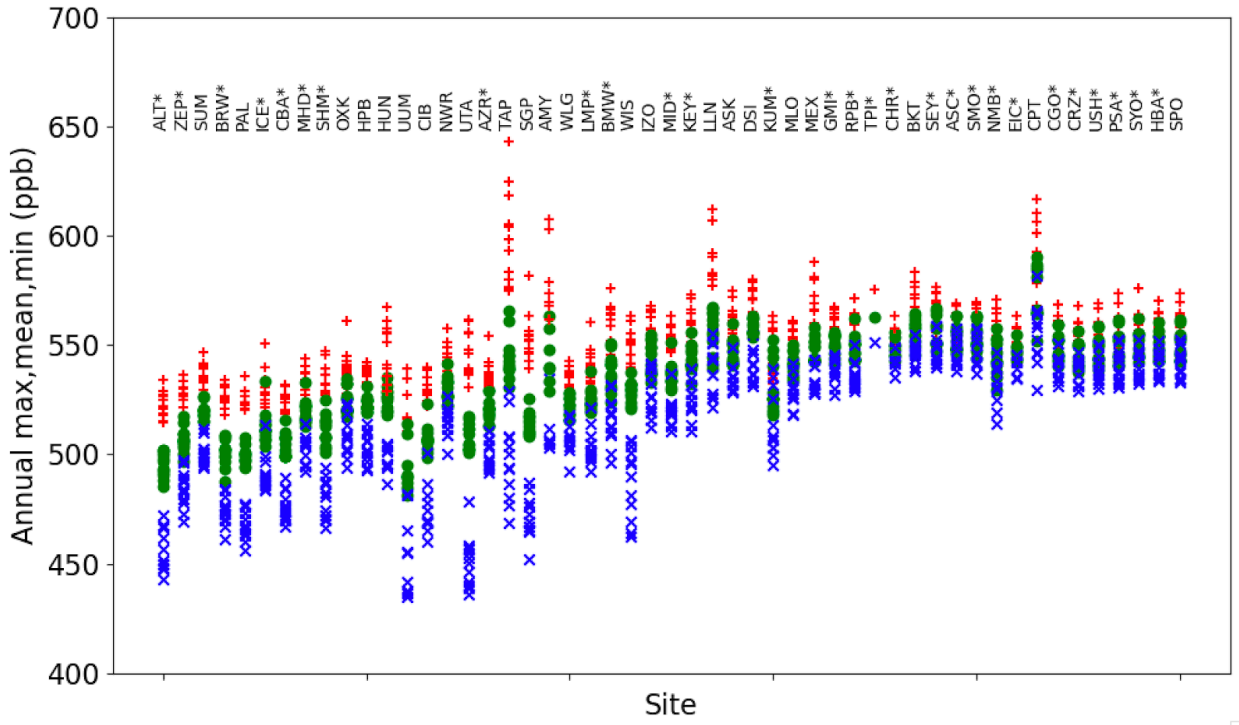


Figure 10. $H_2$ time series at the NOAA Baseline Atmospheric Observatories

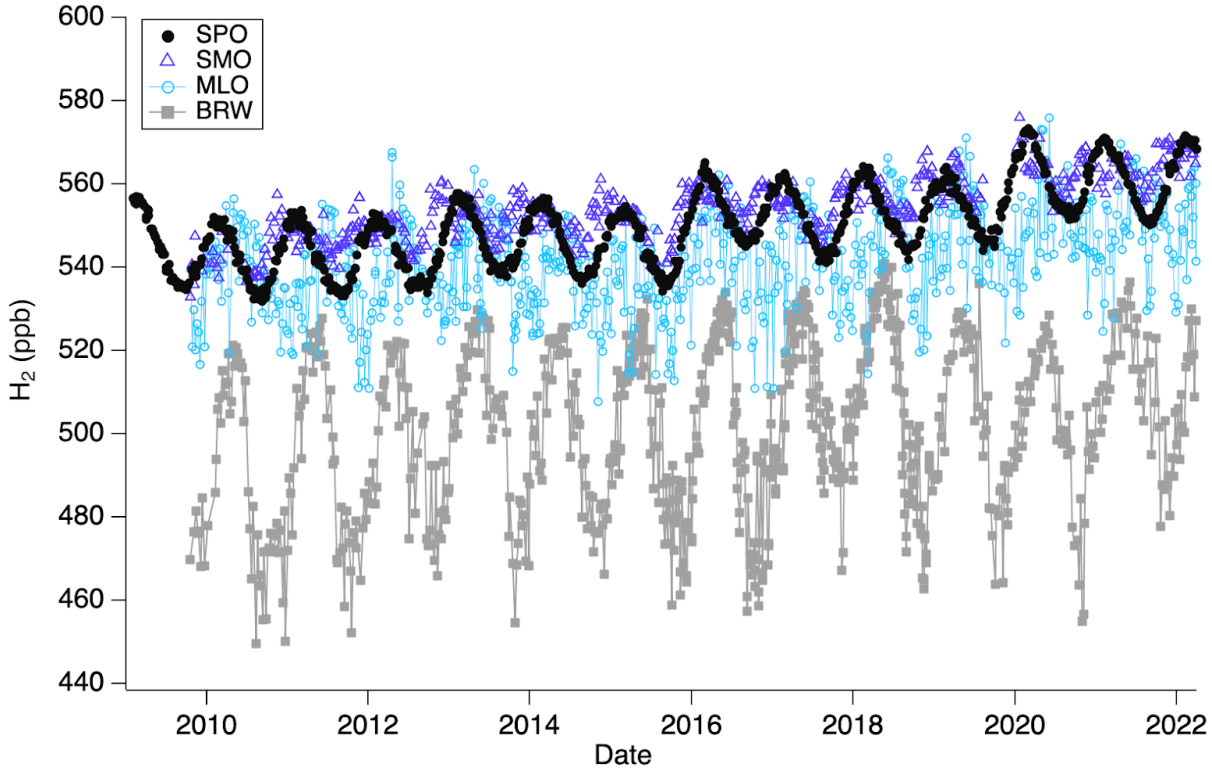

Figure 11: 2010-2021 marine boundary layer $H_2$ meridional gradient. Y-axis is the sine of latitude.

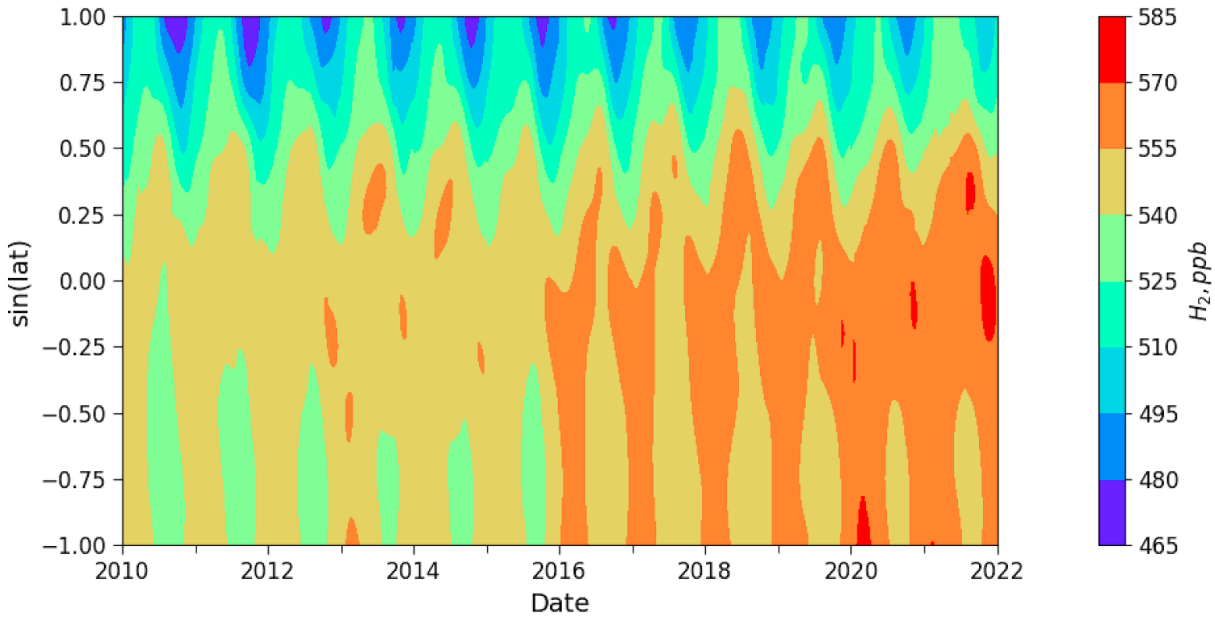

Figure 12: 2010-2021 marine boundary layer global mean and zonal mean $H_2$ anomaly (black line) and CO anomaly (dashed blue line) time series.